Renewable and Sustainable Energy Reviews 39 (2014) 700–728

Contents lists available at ScienceDirect

Renewable and Sustainable Energy Reviews

journal homepage: www.elsevier.com/locate/rser

State-of-the-art in liquid-to-air membrane energy exchangers (LAMEEs): A comprehensive review

Mohamed R.H. Abdel-Salam *, Gaoming Ge, Melanie Fauchoux, Robert W. Besant, Carey J. Simonson

Department of Mechanical Engineering, University of Saskatchewan, 57 Campus Drive, Saskatoon, SK, Canada S7N 5A9

ARTICLE INFO

Article history:
Received 1 October 2013
Received in revised form
25 May 2014
Accepted 6 July 2014
Available online 6 August 2014

Keywords:
Liquid-to-air membrane energy exchanger (LAMEE)
Liquid desiccant
Semi-permeable membrane
Dehumidification
Regeneration
Effectiveness

ABSTRACT

Buildings are responsible for a significant portion of the global energy consumption. In particular, heating, ventilation, and air-conditioning (HVAC) systems in buildings consume significant amounts of energy. Liquid desiccant dehumidification and energy recovery are effective energy conservation technologies in HVAC systems. Direct-contact liquid desiccant air-conditioning systems have the risk of carry-over of aerosol droplets to the supply airstream, which may cause health problems for occupants and corrosion of the ducting system. Liquid-to-air membrane energy exchanger (LAMEE) is a novel semi-permeable membrane-based liquid desiccant energy exchanger, which transfer heat and moisture simultaneously but can eliminate the desiccant solution aerosol carry-over problem. Two LAMEEs can also be used to constitute a run-around membrane energy exchanger (RAMEE) system to recover heat and moisture from exhaust air in buildings. In the past decade, research and development of LAMEEs has been very active to show that high effectiveness is possible. This paper presents a comprehensive review of the design and performance of LAMEEs.

Contents

* Corresponding author. Tel.: +1 306 966 5476; fax: +1 306 966 5427.
E-mail address: moa030@mail.usask.ca (M.R.H. Abdel-Salam).

http://dx.doi.org/10.1016/j.rser.2014.07.022
1364-0321/

1. Introduction

Energy is the engine for human activities, development, and sustainability. Currently, fossil fuels dominate the global energy generation. The world energy consumption increased by 38% between 1998 and 2011 [1,2]. Energy consumption in the Mediterranean region increased by more than three times between 1980 and 2005 [3] and in Canada increased by 23%, between 1990 and 2010 [4]. It is predicted that the energy demand will increase from 87.4 million barrel/day in 2011 to 99.7 million barrel/day in 2035, which may cause petroleum oil prices to increase from $125/barrel in 2011 to more than $215/barrel in 2035 [5]. At the same time, decades of exponential global atmospheric carbon dioxide and ocean acidification increases is likely to cause a dramatic shift and need to conserve energy and reduce fossil fuel use. Buildings account for around 40% of the total global energy consumption [6–8]. Heating, ventilation, and air conditioning (HVAC) systems consume 55% of the total energy consumed in buildings in Malaysia [9], 40–60% in China [10], and 59% in Canada [4].

2. Ventilation

Ventilation is the continuous replacement of contaminated indoor air with fresh outdoor air and accounts for 30–60% of the total energy consumed in buildings [11]. People spend more than 90% of their time inside buildings [12], therefore sufficient ventilation is important to improve the indoor air quality (IAQ) and thus occupants' health, comfort, and performance. Buildings with insufficient ventilation are characterized by high concentrations of pollutants and occupants may suffer from various problems such as discomfort and health problems (e.g. eye, nose, and throat irritations, asthma, allergy, infections, headaches, dizziness, etc.), which decrease the occupants' productivity [13]. Wyon [8] reported that the performance of the occupants in an office may decrease by up to 6–9% due to poor IAQ. Thus, reducing ventilation rates for the sake of energy savings may add extra costs.

Ventilation energy consumption mainly depends on the difference between indoor and outdoor air conditions, occupation density, and the type of building (hospital, office, house, etc.). Design ventilation rates in modern buildings are higher than those for old buildings due to (1) increased ventilation rates to avoid sick building syndrome, (2) larger amounts of VOCs and TVOCs that are emitted from the materials and furnishings used in modern buildings, and (3) tighter building envelopes designed to reduce energy consumption [11], which also reduce the amount of air infiltration into a building that can dilute the pollutants of indoor air.

In vapor compression HVAC technologies, the moisture (latent load) in the ventilation air and indoor air, is reduced by cooling the supply air to a temperature lower than its dew point temperature; thereafter the supply air is reheated to a comfortable supply temperature. In this process, a significant amount of energy is consumed to condense the water vapor out of the air and then reheat the process air. Moreover, during the condensation process, water vapor in the process air is converted to water droplets on the cooling coil, which may re-evaporate in the cooling coil and thus reduce the indoor air quality and increase the supply air humidity.

3. Ventilation energy recovery

During recent years, comprehensive studies [14–25] have been carried out on reducing cooling and heating energy consumption in buildings. Ventilation energy recovery has been considered a key technology for reducing the energy consumption of buildings. Much effort has been spent to find effective technologies to recover as much energy as possible without reducing the indoor air quality. As a means of reducing the energy consumption required to remove the latent load, air-to-air membrane energy exchangers have been comprehensively studied [26–48]. The major difference between these membrane exchangers and traditional sensible exchangers is that the metal plate in a sensible exchanger is replaced by a semi-permeable membrane in a membrane exchanger. A semi-permeable membrane is permeable to heat and water vapor but impermeable to liquids for small pressure differences. In air-to-air membrane energy exchangers, heat and moisture transfer between the supply and exhaust airstreams through the membrane. Air-to-air membrane energy exchangers are efficient for energy recovery and significantly reduce HVAC energy consumption [49–55]. Zhang and Niu [51] reported that in hot and humid climates such as Hong Kong, installing an air-to-air membrane energy recovery ventilator reduced the annual total cooling and ventilation energy consumptions by 12% and 58%, respectively, whereas installing a sensible recovery ventilator saved only 2% and 10%. However, some problems still exist, for example the exhaust and supply airstreams must be adjacent to each other, consequently air-to-air membrane exchangers may not be suitable for some applications, especially for retrofitting existing buildings.

4. Liquid desiccant energy exchangers

Using liquid desiccant solutions for air dehumidification is not new technology. Comprehensive research has been conducted on

Nomenclature*Acronyms*

ACH	Air Changes per Hour
AHRI	Air Conditioning, Heating and Refrigeration Institute
EPS	Enthalpy Pump System
HVAC	Heating, Ventilation, and Air Conditioning
IAQ	Indoor Air Quality
LAMEE	Liquid to Air Membrane Energy Exchanger
RAMEE	Run-Around Membrane Energy Exchanger
TVOCs	Total Volatile Organic Compounds
VOCs	Volatile Organic Compounds

Symbols

A	membrane surface area (m^2)
A_v	packing density (m^2/m^3)
a	shell width (m), constant in correlation
b	shell height (m)
C	heat capacity rate (W/K), constant in correlation
Cr^*	ratio between solution and air heat capacity rates
c_p	specific heat capacity (J/kg K)
D_o	shell diameter (m)
D_{vm}	moisture diffusivity in the membrane (m^2/s)
d	fiber diameter (m)
E	modulus of elasticity (Pa)
f	friction factor
Gr	Grashof number
H^*	operating condition factor
ΔH	difference in total enthalpy per mass of dry air (J/kg_{air})
$h_{m,air}$	convective mass transfer coefficient of the airside (kg/m^2 s)
h	convective heat transfer coefficient (W/m^2 K)
h_v	evaporation heat of vapor (kJ/kg)
k	thermal conductivity (W/m K)
k_m	membrane water vapor permeability (kg/m s)
Le	Lewis number
m^*_{Lat}	dimensionless latent heat ratio
$\dot{m}_{rr}$	moisture removal rate (kg_v/s)
$\dot{m}$	mass flow rate (kg/s)
m_v	moisture emission rate (kg/m^2 s)
NTU	number of heat transfer units
NTU_m	number of mass transfer units
n_{fr}	number of fibers
P	pressure (Pa)
p_w	vapor partial pressure (Pa)
r	radius (m)
Re	Reynolds number
Ri	Richardson number
Sh	Sherwood number
Sh_m	mean Sherwood number
Sc	Schmidt number
S_T	transverse pitch (m)
S_L	longitudinal pitch (m)
T	temperature (°C)
U	overall heat transfer coefficient (W/m^2 K)
U_m	overall mass transfer coefficient (kg/m^2 s)
V	volumetric flow rate (m^3/s)
W	humidity ratio (kg_v/kg_{air})

Greek letters

β	tangential direction
δ	membrane thickness (m)
ε	effectiveness, membrane porosity
ξ	vapor resistance factor of the membrane
ρ	density (kg/m^3)
τ	tortuosity factor
ϕ	packing fraction

Superscript

b	constant in correlation (m)
m	constant in correlation

Subscript

1	membrane surface on airside
2	membrane surface on solution side
air	air
in	inlet
lat	latent
mem	membrane
min	minimum
o	outer
out	outlet
pol	polymer
sen	sensible
sol	solution
tot	total
v	vapor
w	water

Chemical symbols

$Ca(NO_3)_2$	Calcium nitrates
CO	Carbon monoxide
CO_2	Carbon dioxide
KCOOH	Potassium formate
LiCl	Lithium chloride
$MgCl_2$	Magnesium chloride
NO_x	Nitrogen oxides
SO_x	Sulfur oxides

direct-contact liquid desiccant dehumidification systems [56–77]. It was found that direct-contact liquid desiccant dehumidification systems can reduce the energy consumption by up to 26–80% compared to the traditional vapor compression air-conditioning systems in hot humid climates [77].

In direct-contact liquid desiccant dehumidification systems, two packed beds are employed as a dehumidifier and a regenerator. A liquid desiccant solution is sprayed through the bed and comes in direct contact with the process air, which is passed through the bed. During the dehumidification process, the warm and humid outdoor air enters the dehumidifier and comes in direct contact with the sprayed desiccant solution. The vapor pressure gradient between the air and desiccant solution results in heat and moisture to transfer from the warm and humid air to the desiccant solution. The diluted desiccant solution that leaves the dehumidifier is heated and pumped to the regenerator, where heat and water vapor are transferred from the diluted desiccant solution to ambient air and the diluted desiccant solution is regenerated. The system efficiency depends on various parameters (e.g. packing density, bed length, air inlet temperature, desiccant

solution inlet temperature, desiccant solution type, desiccant solution concentration, air and desiccant solution flow rates, etc.) [57–59,71].

It should be mentioned that a main concern about direct-contact liquid desiccant systems is the carry-over problem where some desiccant solution droplets are carried out by the process air, which can affect people's health and can cause corrosion in the ducting system. Furthermore, these systems are characterized by high air pressure drops which increase the operating costs. Liquid-to-air membrane energy exchangers (LAMEEs), which use a semi-permeable membrane to separate the process air and the desiccant solution streams, eliminate the problem of desiccant droplet carry-over associated with direct-contact liquid desiccant energy exchangers.

Liquid desiccant dehumidification and energy recovery are two important technologies to effectively reduce the energy consumption of building HVAC systems. During recent years, several surveys have been conducted on heat and energy recovery techniques in buildings. Mardiana-Idayu and Riffat [78], Alonso et al. [79], Zhang [80], and Ge et al. [81] reviewed the different heat/energy recovery technologies for building applications, whereas Mohammad et al. [77,82] reviewed the liquid desiccant air-conditioning systems. A review of the applications, energy savings, economics and environmental impacts of LAMEEs for HVAC energy recovery in buildings and automobiles is presented by the authors in [83].

For the first time, a comprehensive review of the design, performance, and development of LAMEEs for energy recovery and air dehumidification in building HVAC systems is presented in the current review paper. Excluding patents and commercial developments, Fig. 1 shows the annual number of published studies on LAMEEs and their applications. The first study on LAMEEs was published in 1996, thereafter few studies were conducted until 2010. Starting in 2011, the number of works increased significantly. Fig. 2 shows that 58% of the published works were performed in Canada, 21% in China, and 20% in Italy.

5. Types of LAMEEs

5.1. Flat-plate LAMEE

The structure of a flat-plate LAMEE is similar to a parallel-plate heat exchanger. The main difference is that the metal plate that separates the two fluids is replaced by a semi-permeable membrane. Fig. 3 shows an example of the flat-plate LAMEE structure. It is composed of several air and liquid channels separated by semi-permeable membranes. Heat and moisture transfer simultaneously between the air and liquid desiccant solution through the semi-permeable membrane. Since the pressure on the liquid side is much higher than on the airside during normal operation conditions, support grids are used to support the membrane from deflecting into the air channel.

As shown in Fig. 4, air and liquid flow configurations inside the flat-plate LAMEE can be counter-flow, cross-flow or counter-cross-flow. Fig. 4a shows a counter-flow configuration where the direction of the airflow is opposite to the liquid flow. Fig. 4b shows a cross-flow configuration where the direction of liquid flow is perpendicular to the airflow. Exchangers with a counter-flow configuration are known to have higher effectiveness than those with a cross-flow configuration [85], however it is difficult to manufacture headers that allow adjacent air and solution inlets and outlets. Consequently, a counter-cross-flow configuration, which is a combination between the cross-flow and counter-flow configurations, was proposed by Vali et al. [86]. As shown in Fig. 4c, in a counter-cross-flow configuration, the solution flow is

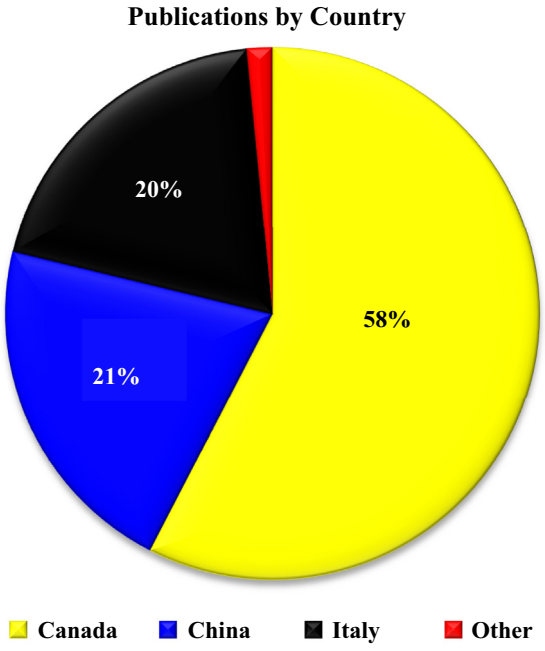

Fig. 2. Publications relating to liquid-to-air membrane energy exchangers by country.

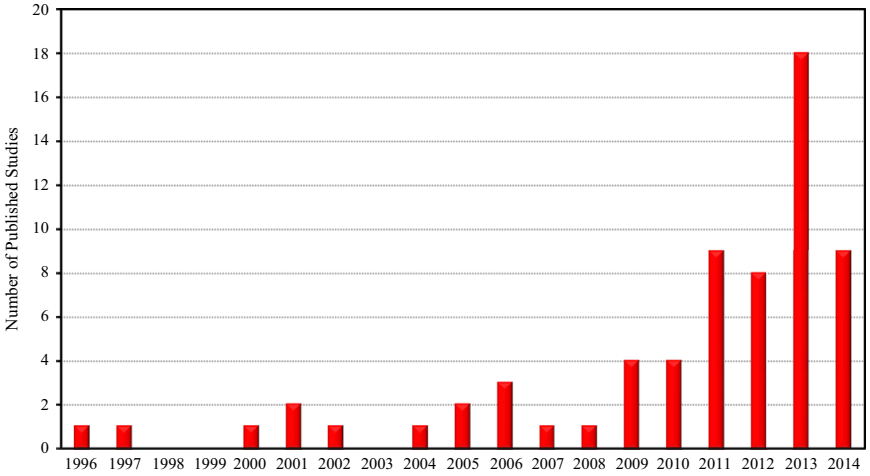

Fig. 1. Number of publications relating to liquid-to-air membrane energy exchangers by year.

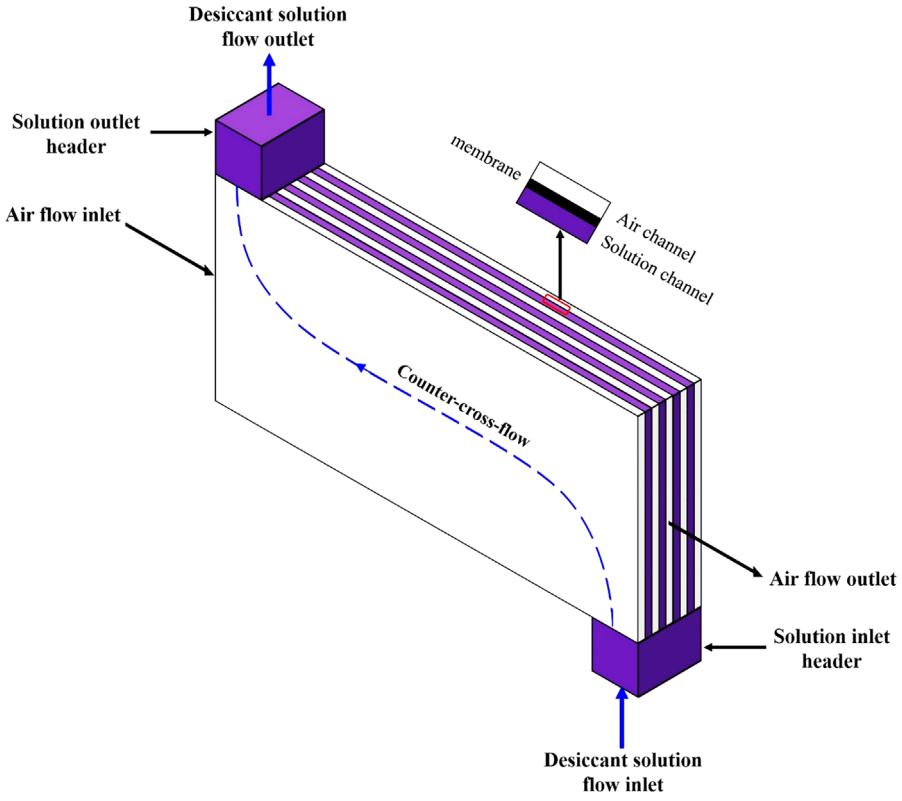

Fig. 3. Structure of a flat-plate LAMEE [83].

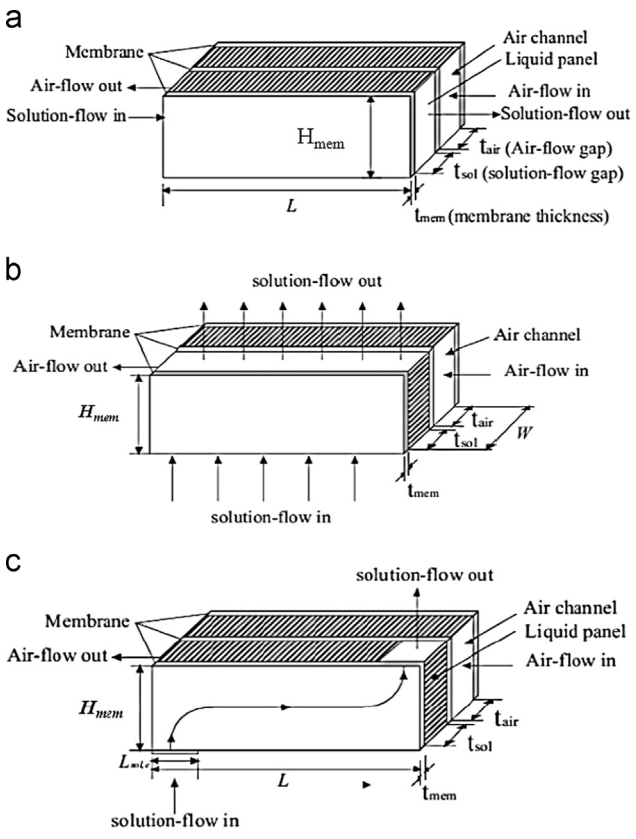

Fig. 4. Flow configurations of air and liquid in (a) a counter-flow LAMEE, (b) a cross-flow LAMEE, and (c) a counter-cross-flow LAMEE [84].

counter to the airflow for more than 90% of the LAMEE's length, and is perpendicular to the airflow near the inlet and outlet headers. As noted in [87], flat-plate LAMEEs are characterized by high heat and mass transfer surface areas with typical values of 800 m^2/m^3 and values as high as 2,000 m^2/m^3 [88].

5.2. Hollow-fiber LAMEE

Fig. 5 shows a typical configuration of a hollow-fiber LAMEE. Its structure is similar to a shell-and-tube heat exchanger but the metal tubes are replaced with hollow fiber semi-permeable membranes that allow simultaneous heat and moisture transfer between the working fluids. Fig. 6 shows an end view photograph of a hollow-fiber LAMEE showing how the hollow fiber membranes are supported on the tube end plate. The air and liquid flow configurations inside the hollow-fiber LAMEE can be counter-flow or cross-flow, where the liquid flows inside the hollow fibers and the air flows around the fibers. Hollow fibers can be either staggered or aligned with the flow [89–91]. As noted in [87], hollow-fiber LAMEEs are characterized by very high heat and mass transfer surface area with typical values of 2000 m^2/m^3 and values as high as 30,000 m^2/m^3 [88]. The number of hollow fibers can vary between 200 [89] and 12,000 [90] in one LAMEE.

6. Evaluation of LAMEE performance

6.1. Effectiveness (ε)

Effectiveness is the most important parameter for evaluating the performance of an exchanger [92]. For energy exchangers, there are three types of effectiveness; sensible, latent, and total.

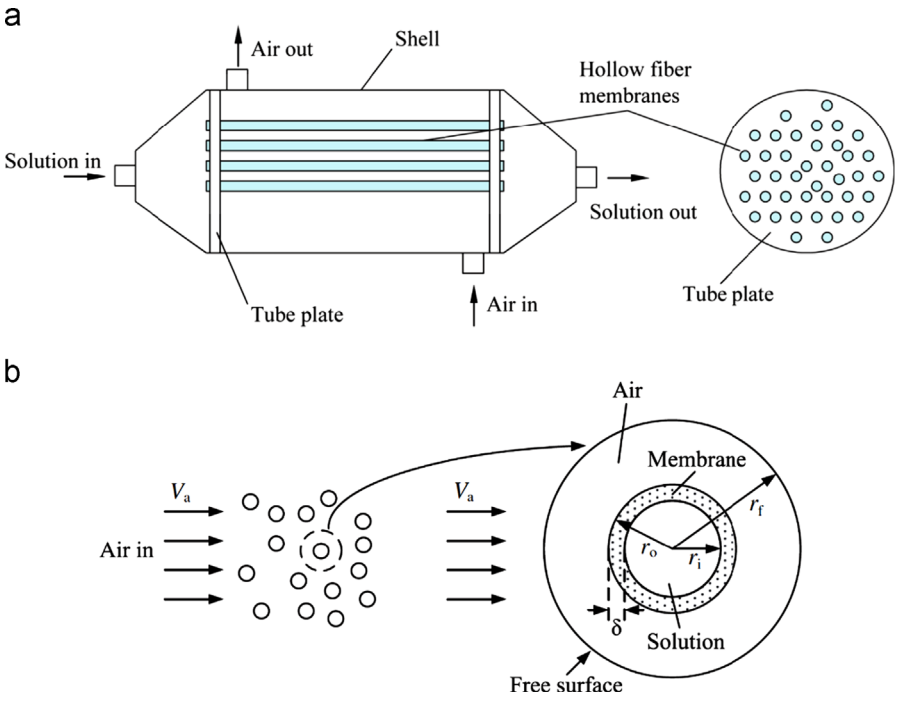

Fig. 5. (a) Structure of a hollow-fiber LAMEE [89], and (b) a detailed schematic of a single hollow fiber [90].

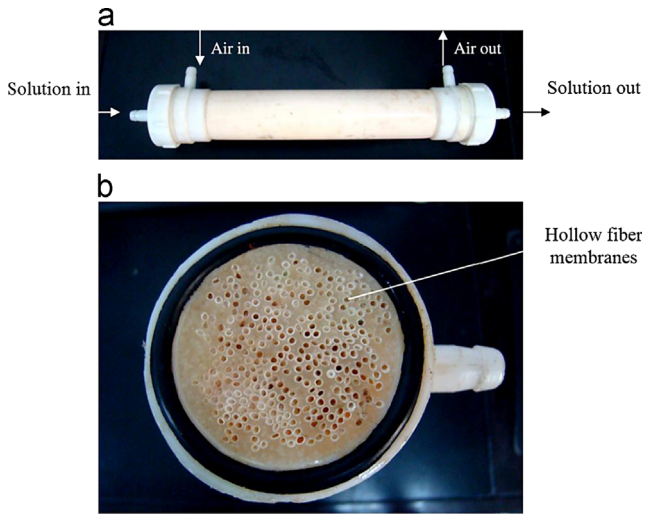

Fig. 6. (a) Photograph of a hollow-fiber LAMEE, and (b) an end view of the hollow fibers inside the LAMEE [91].

Sensible effectiveness (ε_{sen}) is the ratio between the actual and the maximum possible rates of sensible heat transfer inside the exchanger. Latent effectiveness (ε_{lat}) is the ratio between the actual and the maximum possible rates of moisture (latent energy) transfer inside the exchanger. The total effectiveness (ε_{tot}) is the ratio between the actual and the maximum possible rates of energy transfer (enthalpy) inside the exchanger. When the capacitance rate of the desiccant solution is higher than the air ($Cr^* \geq 1$), the sensible, latent and total effectivenesses can be calculated by Eqs. (1)–(3) [93]; respectively.

$$\varepsilon_{sen} = \frac{T_{air,in} - T_{air,out}}{T_{air,in} - T_{sol,in}} \tag{1}$$

$$\varepsilon_{lat} = \frac{W_{air,in} - W_{air,out}}{W_{air,in} - W_{sol,in}} \tag{2}$$

$$\varepsilon_{tot} = \frac{\varepsilon_{Sen} + H^* \varepsilon_{Lat}}{1 + H^*} \tag{3}$$

where $T_{air,in}$ is the air temperature at the exchanger inlet (°C), $T_{air,out}$ is the air temperature at the exchanger outlet (°C), $T_{sol,in}$ is the desiccant solution temperature at the exchanger inlet (°C), $W_{air,in}$ is the humidity ratio of the air at the exchanger inlet (kg/kg), $W_{air,out}$ is the humidity ratio of the air at the exchanger outlet (kg/kg), $W_{sol,in}$ is the humidity ratio of the desiccant solution at the exchanger inlet (kg/kg), and H^* is the operating factor.

6.2. Dehumidification/humidification rate (moisture removal rate) ($\dot{m}_{rr}$)

The mass transfer rate is another important indicator for the performance of a LAMEE. It is the mass transfer rate of moisture between the air and the desiccant solution.

$$\dot{m}_{rr} = \dot{m}_{air} \, |W_{air,out} - W_{air,in}| \tag{4}$$

where $\dot{m}_{air}$ is the mass flow rate of the dry air (kg/s).

6.3. Designand operating parameters

The performance (i.e. effectiveness and moisture removal rate) of a LAMEE significantly depends on several parameters.

6.3.1. Number of heat transfer units (NTU)

The number of heat transfer units has a significant effect on the sensible effectiveness of a LAMEE. The sensible effectiveness of a LAMEE increases as *NTU* increases.

$$NTU = \frac{UA}{C_{\min}} \tag{5}$$

$$U = \left[\frac{1}{h_{air}} + \frac{\delta}{k_{mem}} + \frac{1}{h_{sol}} \right]^{-1} \tag{6}$$

where U is the overall heat transfer coefficient (W/m^2 K), A is the membrane surface area (m^2), C_{min} is the minimum heat capacity rate of air and desiccant solution flows (W/K), h_{air} is the convective

heat transfer coefficient of the air (W/m^2 K), δ is the membrane thickness (m), k_{mem} is the membrane thermal conductivity (W/m K), and h_{sol} is the convective heat transfer coefficient of the desiccant solution (W/m^2 K).

6.3.2. Number of mass transfer units (NTU_m)

The number of mass transfer units has a significant effect on the latent effectiveness of a LAMEE. The latent effectiveness increases as NTU_m increases.

$$NTU_m = \frac{U_m A}{\dot{m}_{\min}} \tag{7}$$

$$U_m = \left[\frac{1}{h_{m,\text{air}}} + \frac{\delta}{k_m} + \frac{1}{h_{m,sol}}\right]^{-1} \tag{8}$$

where U_m is the overall mass transfer coefficient (kg/m^2 s), $\dot{m}_{\min}$ is the minimum mass flow rate of air and desiccant solution flows (kg/s), $h_{m,air}$ is the convective mass transfer coefficient of the air (kg/m^2 s), and k_m is the membrane water vapor permeability (kg/m s). Hemingson [94] has showed that the convective mass transfer coefficient of the desiccant solution ($h_{m,sol}$) is much higher than that of the air ($h_{m,air}$), and thus ($1/h_{m,sol}$) can be neglected in Eq. (8).

6.3.3. Ratio of heat capacity rates (Cr^*)

The effectiveness of a LAMEE strongly depends on the ratio of heat capacity rates between the desiccant solution and air flows.

$$C_r^* = \frac{C_{sol}}{C_{air}} = \frac{\dot{m}_{sol}\, c_{p,sol}}{\dot{m}_{air}\, c_{p,air}} \tag{9}$$

where C_{sol} is the heat capacity rate of the desiccant solution (W/K), C_{air} is the heat capacity rate of the air (W/K), $\dot{m}_{sol}$ is the desiccant solution mass flow rate (kg/s), $\dot{m}_{air}$ is the air mass flow rate (kg/s), $c_{p,sol}$ is the specific heat capacity of the desiccant solution (J/kg K), and $c_{p,air}$ is the specific heat capacity of the air (J/kg K).

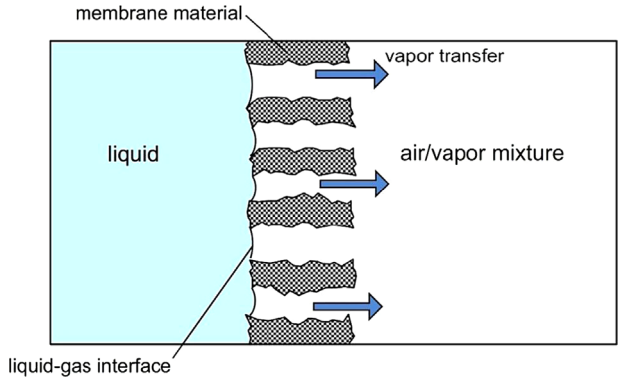

Fig. 7. Schematic of heat and water vapor transfer processes through a semi-permeable membrane [97].

6.3.4. Operating factor (H^*)

The operating factor is a dimensionless number that describes the ratio between the difference in latent energy and the difference in sensible energy between the air and the desiccant solution at the LAMEE inlets [93].

$$H^* = \frac{\Delta H_{Lat}}{\Delta H_{Sen}} \approx 2500\, \frac{W_{air,in} - W_{sol,in}}{T_{air,in} - T_{sol,in}} \tag{10}$$

6.3.5. Moisture emission rate (m_v)

The moisture flux through the membrane [91].

$$m_v = \rho_{air} D_{vm} \frac{W_{mem,1} - W_{mem,2}}{\delta} \tag{11}$$

where ρ_{air} is the air density (kg/m^3), D_{vm} is the moisture diffusivity in the membrane (m^2/s), $W_{mem,1}$ is the humidity ratio of the membrane on the airside (g/kg), and $W_{mem,2}$ is the humidity ratio of the membrane on the solution side (g/kg).

6.3.6. Latent heat ratio (m^*_{Lat})

For the air humidification process using water, Zhang [95] introcuced a dimensionless *latent heat ratio* that shows how the water temperature is affected by the moisture evaporation heat.

$$m^*_{Lat} = \frac{\rho_{air} V_{air} h_v (W_{w,in} - W_{air,in})}{\rho_w V_w c_{p,w} (T_{w,in} - T_{air,in})} \tag{12}$$

where h_v is the evaporation heat of vapor (kJ/kg).

The following parameters characterize the structure of a hollow-fiber LAMEE:

6.3.7. Packing density (A_v)

The ratio between the actual mass transfer area and the exchanger unit volume is referred to as the packing density [96].

$$A_V = \frac{4\, n_{fr}\, d_o}{D_o^2} \tag{13}$$

where n_{fr} is the number of fibers, d_o is the outer diameter of a single hollow fiber (m), and D_o is the shell diameter (m).

6.3.8. Packing fraction (ϕ)

The packing fraction gives an indication of the average area occupied by the hollow fibers in a rectangular shell [90].

$$\phi = \frac{n_{fr}\, \pi\, r_o^2}{a\, b} \tag{14}$$

where r_o is the outer radius of a single hollow fiber (m), a is the shell width (m), and b is the shell height (m).

Table 1
Comparison between different commercial membranes [113].

Membrane	Membrane polymer	Cost ($US/ft^2)	Pore size (μm)	Porosity (%)	LPP (kPa)	VDR (s/m)	E (MPa)
Propore™	Polypropylene	0.1	< 1	–	> 82	158	17
Tredegar #2	Polypropylene	–	–	–	> 82	5,793	45
Aptra™ RKW	Polypropylene	0.35	0.2	60	–	385	–
Porex® PM6M	Polytetrafluoroethylene	40	1–2	35–45	–	84	16
Porex® PM3V	Polytetrafluoroethylene	40	5	40	49	57	12
Porex® X-7744	Polypropylene	5	7	35–45	15	102	–
Porex® X-4904	Polypropylene	5	2	35–45	–	40	–
Japanese Tyvek®	High density polypropylene	0.15	2–15	45	19	329	382
Tyvek® 1025B	High density polypropylene	0.15	2–15	45	16	245	–
Tyvek® 1059B	High density polypropylene	0.15	2–15	45	17	215	–
AY Tech Laminant	Polytetrafluoroethylene	3.27	0.3	85	> 82	97	387

7. Membranes

The semi-permeable membrane is considered to be the most important component in a LAMEE. Fig. 7 shows a schematic for the heat and water vapor transfer processes through a semi-permeable membrane. Generally, there are two types of semi-permeable membranes; hydrophobic and hydrophilic. Hydrophobic membranes resist penetration by liquid water and water droplets remain on the surface whereas hydrophilic membranes draw in liquid water and are easily wetted [98]. Hydrophobic membranes are used for LAMEE applications. There are various commercial micro-porous hydrophobic membranes available, such as polypropylene (PP), polyethylene (PE), polytetrafluoroethylene (PTFE), and polyvinylidene fluoride (PVDF) [99]. Other types of membranes, such as composite membranes and composite supported liquid membranes, can also be used in membrane energy exchangers [100–102].

The semi-permeable membrane properties have a significant influence on heat and moisture transfer in the LAMEE. The most important properties are:

1. *Vapor Diffusion Resistance* (*VDR*): the resistance to water vapor diffusion through the membrane. The VDR increases as the membrane thickness increases. The rate of water vapor transfer through the membrane, known as *membrane permeability*, increases as the VDR decreases [103,104]. As well, the permeability of the membrane depends on temperature and humidity [97].
2. *Liquid Penetration Pressure* (*LPP*): the pressure difference at which liquid water will penetrate through the membrane. The LPP increases as the membrane thickness increases [103,104].
3. *Pore Size*: the permeability of the membrane increases as the pore surface area ratio increases. As well, the size of the pores should be as small as possible to prevent liquid transfer through the membrane. Consequently, the optimum pore size is determined by a trade-off between permeability and LPP.
4. *Membrane Porosity* (ε): the ratio between the volume of the pores and the total volume of the membrane [105]. The membrane porosity is calculated by the Smolder–Franken equation [106]

$$\varepsilon = 1 - \frac{\rho_{mem}}{\rho_{pol}} \tag{15}$$

where ρ_{mem} is the average density of the membrane (kg/m^3), and ρ_{pol} is the density of the polymer material (kg/m^3).

5. *Membrane Tortuosity Factor*: an indication of the deviation in the structure of the membrane pores from a straight cylindrical structure normal to the membrane surface [99]. As noted in [107], the membrane tortuosity can be determined from Mackie–Meares correlation [108]

$$\tau = \frac{(2-\varepsilon)^2}{\varepsilon} \tag{16}$$

where τ is the tortuosity factor and ε is the membrane porosity.

6. *Modulus of Elasticity* (*E*): the ratio between the stress and strain of the membrane when subjected to a certain force. High values of *E* imply that the membrane deflections will be small when subjected to pressure differences between the air and liquid sides.
7. *Thermal Conductivity*: Brandrup and Immergut [109], Harper [110], and Van Kreveleh [111] reported coefficients of thermal conductivity in the ranges of 0.17–0.19 (W/m K) for PVDF (at 296 K); 0.25–0.27 (W/m K) for PTFE (at 296 K); and 0.11–0.16 (W/m K) for PP (at 296 K) [109–112]. The thermal conductivity of the membrane depends on temperature; for instance, the thermal conductivity of PP increases from 0.11–0.16 (W/m K) to 0.2 (W/m K) when the temperature increases from 23 °C to 75 °C [109–112]. It is worth mentioning that the influence of membrane thermal conductivity on a LAMEE's sensible, latent, and total effectivenesses during air humidification and dehumidification is very small and negligible in the flat-plate LAMEEs.

Beriault [113] presented a comparison between different membrane types as shown in Table 1. In conclusion, competitive membranes should be characterized by:

1. High liquid penetration pressure,
2. Low vapor diffusion resistance,
3. High modulus of elasticity,
4. High porosity,
5. Small thermal resistance,
6. High selectivity [114],
7. Small tortuosity factor [99],
8. Ability to sustain high temperatures (i.e. 40–70 °C), especially for applications as a regenerator,
9. Competitive chemical resistance for different fluids (i.e. water and different liquid desiccants) [99],
10. High durability,
11. High fouling resistance especially for the side contacting the process air [99] and
12. Cost effective.

8. Development of LAMEEs

In this section, the work that has been done on the flat-plate and hollow-fiber LAMEEs will be presented and discussed

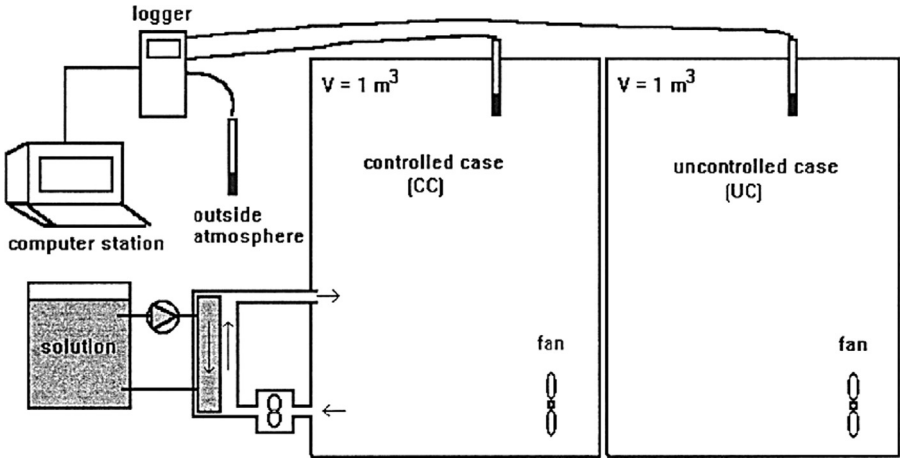

Fig. 8. Schematic diagram for the experimental setup [115].

according to the year of publication. Some researchers used the term "contactor" to refer to the LAMEE, however we will replace it with "LAMEE" to avoid any confusion.

8.1. The flat-plate LAMEE

8.1.1. Steady-state performance

Research on flat-plate LAMEEs started as early as 1996 when Isetti et al. [115] presented a novel technique to control the indoor air relative humidity inside a museum display case by using a hydrophobic membrane that allowed simultaneous heat and water vapor transfer between air and a hygroscopic solution. The performance of the proposed technology was experimentally evaluated by comparing it with an uncontrolled display case. Fig. 8 shows the experimental setup where LiCl was employed as the hygroscopic solution and a commercial micro-porous PTFE membrane was used as a contact surface between the air and the LiCl solution. Fig. 9 shows that when LiCl solution with a concentration of 20% was employed for controlling the indoor air relative humidity, the proposed technology was able to keep the relative humidity of the indoor air near 60% for 3 months even under sudden sharp variations in the outdoor air relative

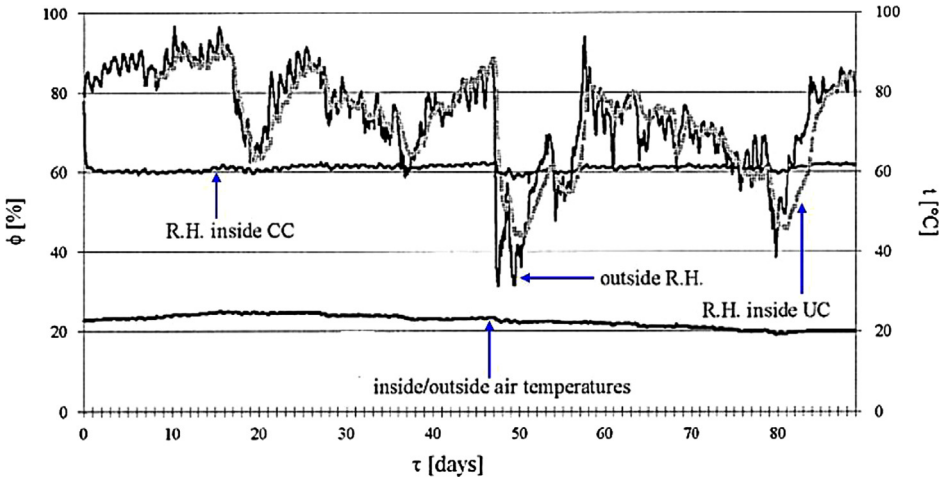

Fig. 9. Variation of the indoor air relative humidity using a 20% LiCl solution over a 90 day period [115].

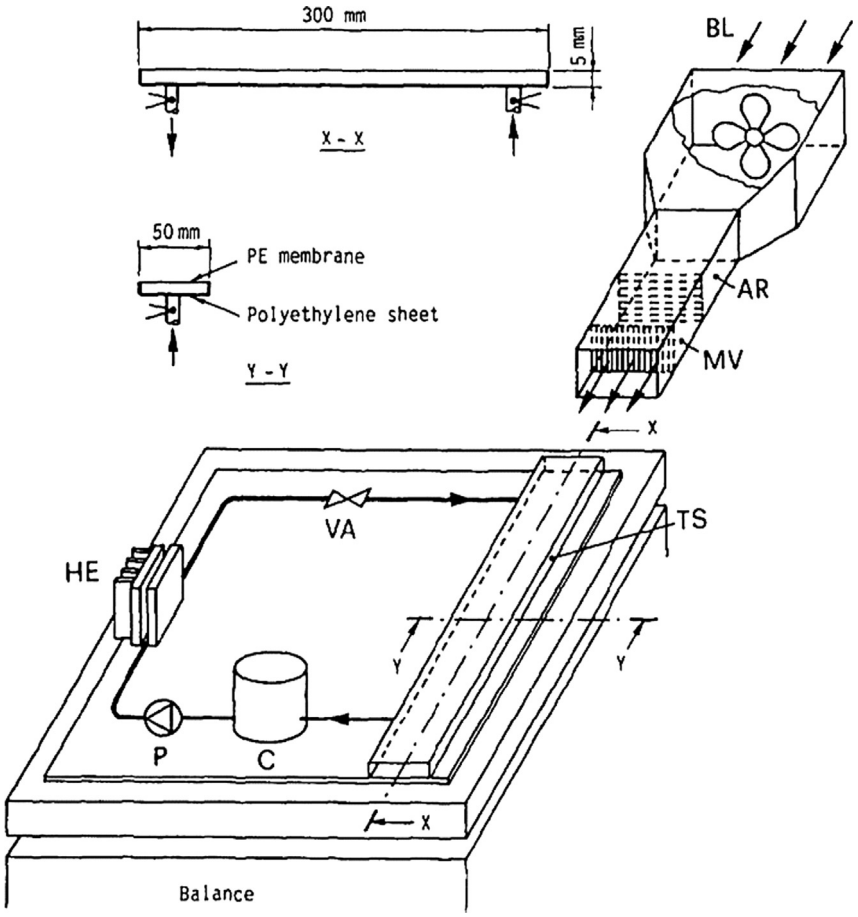

Fig. 10. The experimental setup of Isetti et al. [87].

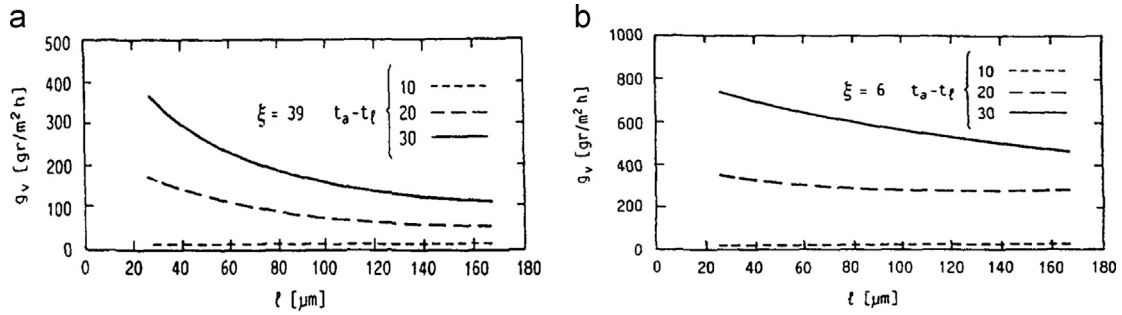

Fig. 11. Effect of the membrane thickness and temperature gradient across the membrane on the vapor mass flux for (a) a PE membrane (ξ=39), and (b) a PTFE membrane (ξ=6) [87].

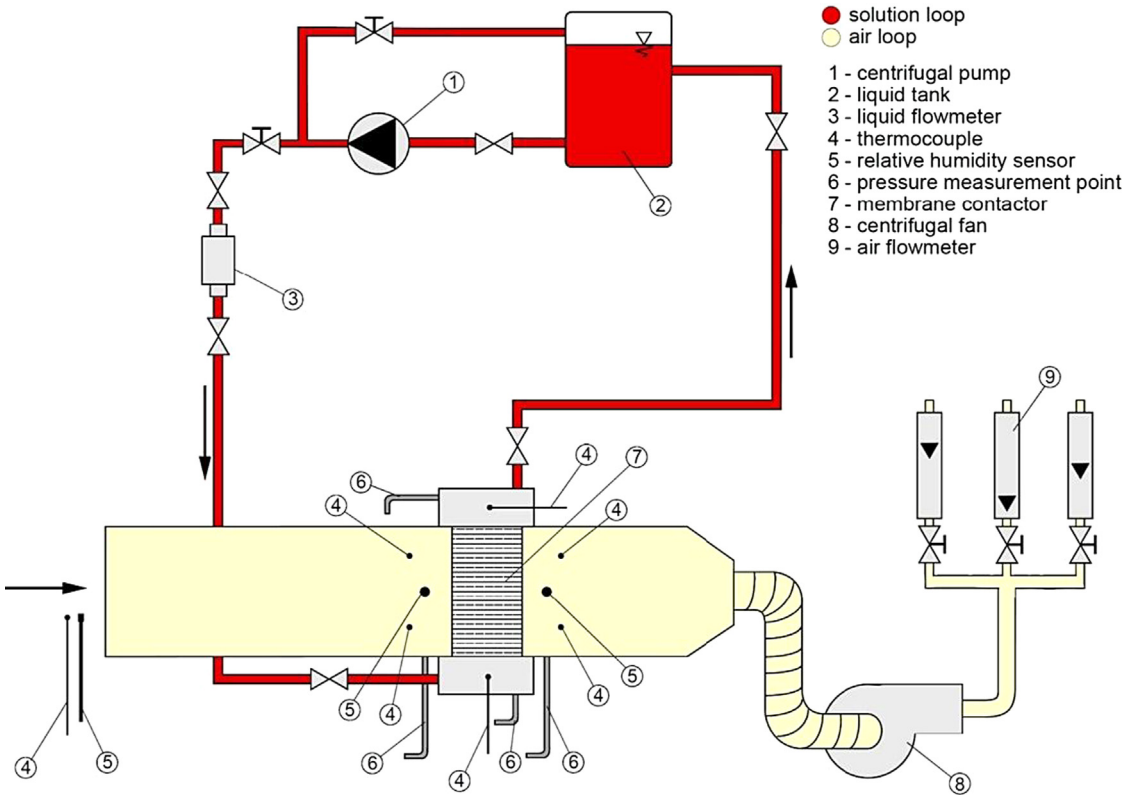

Fig. 12. The experimental setup of Bergero et al. [116].

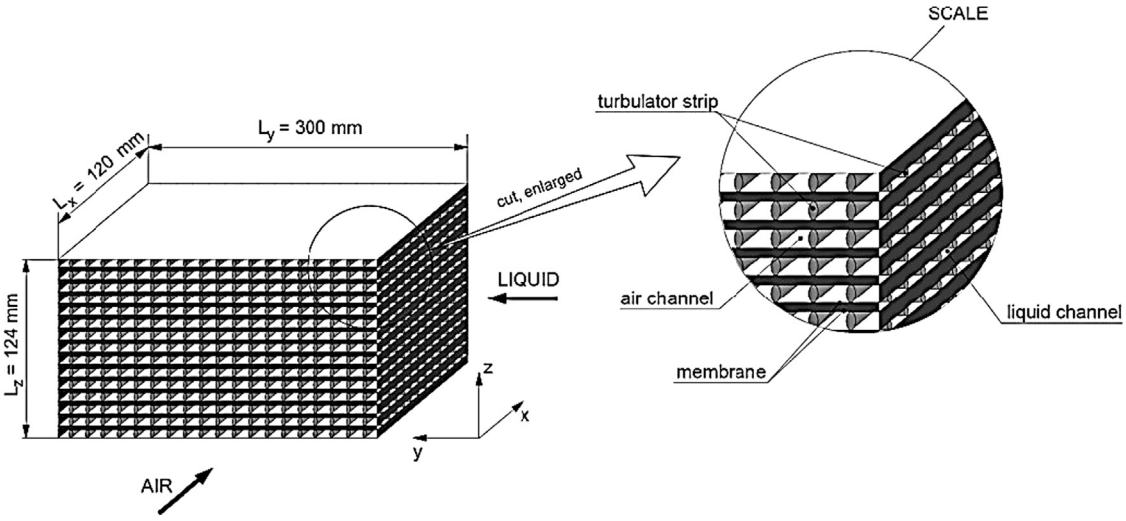

Fig. 13. LAMEE structure and dimensions [116].

humidity. Another experiment was performed over a shorter time period (i.e. 4 weeks) and with a smaller amount of LiCl solution at a concentration of 31%; the results confirmed the ability of the proposed technology to control the indoor air relative humidity. These results motivated further research on LAMEE performance.

Isetti et al. [87] developed a theoretical equation to explain the dependency of the vapor mass flux across a hydrophobic membrane on the design and operating parameters, and validated this correlation with experimental results. Fig. 10 shows the test-rig used in these experiments. A liquid desiccant solution was pumped from the solution container (C) through a thermoelectric heat exchanger (HE) to control the solution temperature and a valve (VA) to control the solution mass flow rate before it entered the test section (TS). An array of electrical resistance (AR) was used to heat the air and a mixing vane (MV) was used to obtain a constant temperature and velocity of the air at the test section inlet. LiCl solution with a concentration of 42% and $Ca(NO_3)_2$ with a concentration of 56% were used as the desiccant solutions. The experimental results agreed with the theoretical results from the developed equation, consequently, the equation was used to investigate the effect of the design and operating parameters on the vapor mass flux. Fig. 11a and b show that the membrane thickness, membrane vapor resistance factor (ξ), and temperature difference across the membrane have significant influences on the vapor mass flux through the membrane. At high temperature gradients across the membrane, the vapor mass flux increased significantly as the membrane thickness decreased. However, the increase in the vapor mass flux decreased as the temperature gradient across the membrane decreased. The vapor mass flux increased by 2–4 times when the membrane vapor resistance factor decreased from 39 to 6. They found that the vapor mass transfer rate through the membrane is dominated by the resistance of the membrane and the airside boundary layers. During desiccant solution regeneration, the required liquid temperature decreased as the thickness and vapor diffusion resistance of the membrane decreased.

Bergero et al. [116] theoretically and experimentally investigated the performance of a cross-flow LAMEE used for air dehumidification. The experimental apparatus was built at the University of Genoa and is shown in Fig. 12. The membrane was made of PVDF with a thickness of 190 μm. PP turbulator strips were used to support the structure of the LAMEE as shown in Fig. 13. Results showed that the air outlet temperature was 24 °C which was higher than the desiccant solution inlet temperature of 23.5 °C. This phenomenon occurred as a result of the heat of phase change released at the liquid interface during the process of moisture transfer from the air stream to the desiccant solution. They also found that the desiccant solution mass flow rate had a negligible effect on the overall mass flux across the membrane, whereas the mass flux increased as the volumetric air flow rate increased. The theoretical results revealed that the majority of the mass transfer resistance was caused by the membrane (the airside resistance was 10% of the total and the liquid side resistance was negligible) and thus the membrane resistance was identified as the key parameter for enhancing mass transfer.

Bergero and Chiari [117] developed a Simulink model to investigate the ability of a cross-flow LAMEE to reduce the fluctuations of the indoor air relative humidity in confined environments. The LAMEE structure was similar to that in Bergero et al. [116]. The LAMEE was housed inside an energy exchanger unit. The energy exchanger unit and a temperature control device were placed in a 100 m^3 room with a ventilation rate of 0.3 ach. Simulation results showed that the LAMEE was able to significantly reduce the short-term fluctuations in the indoor air relative humidity. Furthermore, increasing the contact surface area between the air and the LiCl solution decreased the fluctuations significantly over short periods but had negligible effect over medium and long periods. Changing the mass of LiCl in the vessel from 10 to 20 kg (i.e. mass solution from 65 to 120 kg) had a negligible effect on the fluctuations control whereas installing a regenerator for desiccant solution regeneration caused a significant reduction in the fluctuations over medium and long periods. It was concluded that the LAMEE is able to achieve a significant reduction in the indoor air relative humidity fluctuations over short periods whereas a significant reduction in the fluctuations over medium and long period can be achieved only if a regeneration system is installed.

Vestrelli [118] developed a Simulink model to compare the LAMEE performance when used as a humidifier and as a dehumidifier. Results showed that when the LAMEE was employed as a dehumidifier, higher vapor flow rates across the membrane were obtained as the solution concentration increased or the solution temperature decreased at the exchanger inlet. On the other hand, when the exchanger was employed as a humidifier, higher vapor flow rates across the membrane were obtained as the solution concentration decreased or solution temperature increased at the exchanger inlet. Experimental work was carried out where LiCl solution was used during the dehumidification experiments and water was used during the humidification experiments. The experimental results agreed with the developed Simulink model.

Research on LAMEEs began at the University of Saskatchewan in 2002 through a NSERC Collaborative Research and Development Grant with Venmar CES Inc. Mathematical/numerical models were developed and published as follows: Fan et al. [119,120] (cross-flow LAMEE), Seyed-Ahmadi et al. [121–123] (transient cross-flow LAMEE), Vali et al. [86,124] (counter-cross-flow LAMEE) and Hemingson et al. [94,125] (improved modeling of moisture transfer resistance between the membrane and solution) and Namvar et al. [126,127] (thermal capacitance of exchanger). LAMEE prototypes have been built and tested by Hemingson [128], Erb et al. [129,130], Mahmud et al. [84,131], Beriault [113], and Moghaddam et al. [132]. Experimental and numerical data have been compared and agreement has often been within the experimental and numerical uncertainties [122,127,130,132].

Ge et al. [133] extended an analytical model for the counter-cross-flow LAMEE based on an analytical solution first created by Zhang [89]. For the sake of simplicity, Ge et al. [133] assumed that the desiccant solution mass flow rate and concentration were constant in the heat and moisture transfer processes. Namvar et al. [126] used a counter-cross-flow prototype [113] to investigate the steady-state performance of the counter-cross-flow LAMEE under AHRI summer operating conditions [134]. Specifications of the LAMEE used in the experiments are given in Table 2. They have

Table 2
Specifications of the Beriault [113] LAMEE prototype [126].

	Parameters	Value
Exchanger	Length (m)	1.218
	Height (m)	0.305
	Number of solution channels	10
	Air channel thickness (mm)	6.35
	Solution channel thickness (mm)	3.17
	Total mass (kg)	28
Membrane	Type	ePTFE-AY Tech
	Thickness (mm)	0.54
	Thermal conductivity (W/m K)	0.334
	Vapor diffusion resistance (s/m)	97

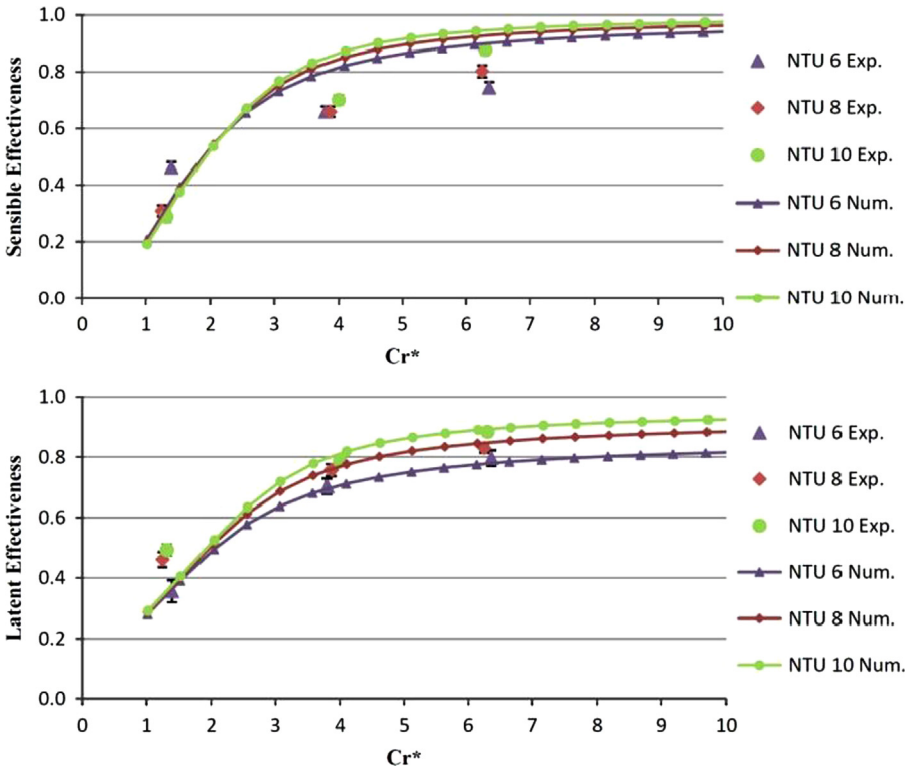

Fig. 14. Comparison of data and simulations for steady-state sensible and latent effectivenesses of the counter-cross-flow LAMEE versus *Cr** under summer operating conditions [127].

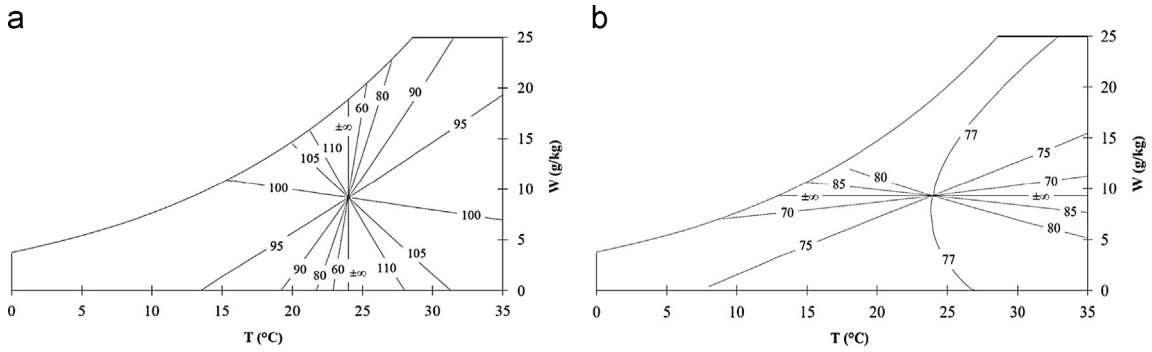

Fig. 15. Simulations of steady-state effectivenesses plotted on the psychrometric chart (a) sensible effectiveness, and (b) latent effectiveness for different outdoor inlet air conditions at $NTU=8$, $Cr^*=6.3$, $T_{sol,in}=24$ °C, and $W_{sol,in}=9.3$ g/kg [127].

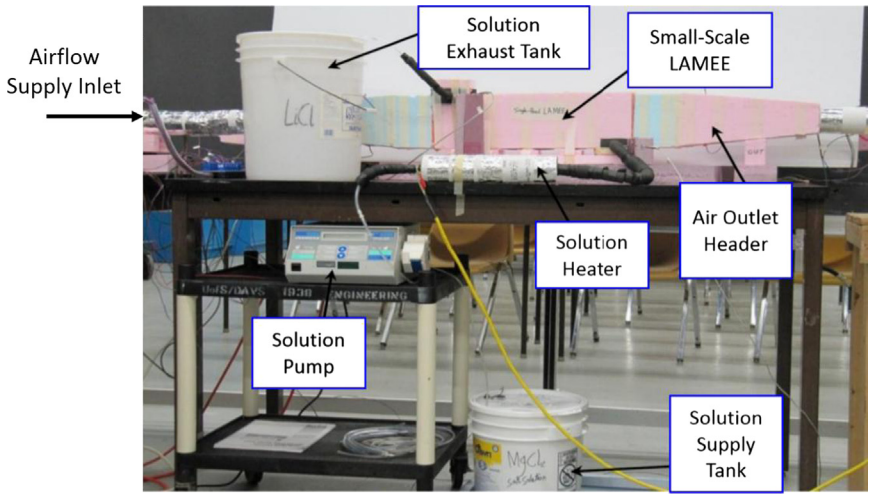

Fig. 16. Photograph of the small-scale LAMEE test setup at the University of Saskatchewan.

compared their experimental results with effectiveness correlations for a single counter-flow heat exchanger from Incropera and Dewitt [135], and with results from Nasif et al. [136], and with the analytical model of Ge et al. [133]. For sensible effectiveness, the results from Incropera and Dewitt [135] were higher than the experimental results. There was a better agreement for latent effectiveness with the results of Nasif et al. [136]. Results from the analytical model of Ge et al. [133] agreed with experimental results at Cr^* of 1.3 but were higher than experimental results at Cr^* equal to 3.9 and 6.3.

In order to get a full map for the counter-cross-flow LAMEE performance, Namvar et al. [127] numerically studied the steady-state performance of the counter-cross-flow LAMEE under various operating conditions. Fig. 14 shows that under summer operating conditions, the sensible and latent effectivenesses increase as *NTU* increases, for a given Cr^* value. *NTU* has a more significant effect on the latent effectiveness than on the sensible effectiveness. Furthermore, the sensible and latent effectivenesses increase as Cr^* increases and Cr^* has a more significant effect on the effectivenesses at Cr^* values between 1 and 5. Fig. 15 shows contour maps of the simulated steady-state sensible and latent effectivenesses on a psychometric chart. Fig. 15a reveals that as the inlet air humidity ratio increases, the sensible effectiveness decreases, if the outdoor air temperature is higher than the desiccant inlet temperature and increases if the desiccant inlet temperature is higher than the outdoor air temperature. Fig. 15b shows that as the inlet air temperature increases, the latent effectiveness decreases, if the outdoor air humidity ratio is higher than the desiccant humidity ratio and increases if the desiccant inlet humidity ratio is higher than the outdoor air humidity ratio. Consequently, the latent effectiveness increases and the sensible effectiveness decreases as H^* increases. In general, the sensible, latent, and total effectivenesses increase as *NTU* and/or Cr^* increase. Effectiveness values over 100% can only be observed in case of sensible effectiveness but not for latent effectiveness in Fig. 15.

Table 3
Specifications of the small-scale LAMEE [132].

Parameter	Value
Exchanger length (m)	0.49
Exchanger aspect ratio	5.2
Exchanger entrance ratio	0.11
Air channel thickness (mm)	5
Solution channel thickness on each panel side (mm)	0.8
Membrane thickness (mm)	0.265

Testing full-scale exchangers is quite expensive and time consuming. An attractive alternative is to test a small-scale model exchanger. Moghaddam et al. [132,137,138,139] conducted several theoretical and experimental studies on a small-scale LAMEE at the University of Saskatchewan. Moghaddam et al. [132] tested the small-scale LAMEE to investigate LAMEE performance for air heating and humidifying (HH), air cooling and humidifying (CH), and air cooling and dehumidifying (CD) using water. Fig. 16 shows a photograph of the small-scale LAMEE prototype and its specifications are given in Table 3. The flow configurations of the air and solution inside the small-scale LAMEE are given in Fig. 17a and the structure is shown in Fig. 17b. In the HH, CH, and CD test processes, a total of nine experiments were conducted at a constant Cr^* of 7 and *NTU* of 2.5, 3.5 and 4.5. Results showed that in the three test processes, the effectivenesses increased with *NTU*. The Enthalpy Pump System (EPS) numerical model developed at the University of Saskatchewan [94,121,124] was modified based on the small-scale LAMEE and was used to develop the sensible and latent effectiveness contour maps superimposed on the psychrometric chart shown in Fig. 18. These contour maps show that the sensible and latent effectivenesses of the small-scale LAMEE depend on the air inlet temperature and humidity ratio and vary from 75% to 120% and 70% to 90%, respectively. A sensible effectiveness greater than 100% occurs when H^* is large or when the phase change energy exceeds the sensible energy by several times. When phase change energy effects are significant, it is noted that sensible energy of inlet and outlet flows will not be conserved in an exchanger that is isolated from its surroundings. The definition of sensible energy effectiveness which was developed for sensible energy does not include any correction for phase change energy.

A LAMEE can be used in different climates (i.e. hot and humid, hot and dry, cold and humid, cold and dry), and can be employed as a dehumidifier, humidifier, or regenerator. These different applications create different directions of heat and mass transfer inside the LAMEE. Moghaddam et al. [137] experimentally and numerically studied the effect of the direction of heat and mass transfer between the air and desiccant solution on the performance of the small-scale LAMEE. The different directions of heat and mass transfer are represented by the cooling and dehumidification, cooling and humidification, heating and dehumidification, and heating and humidification processes. When the heat and mass transfer were in the same direction (i.e. cooling and dehumidifying or heating and humidifying), the sensible effectiveness increased as Cr^* increased whereas when heat and mass transfer

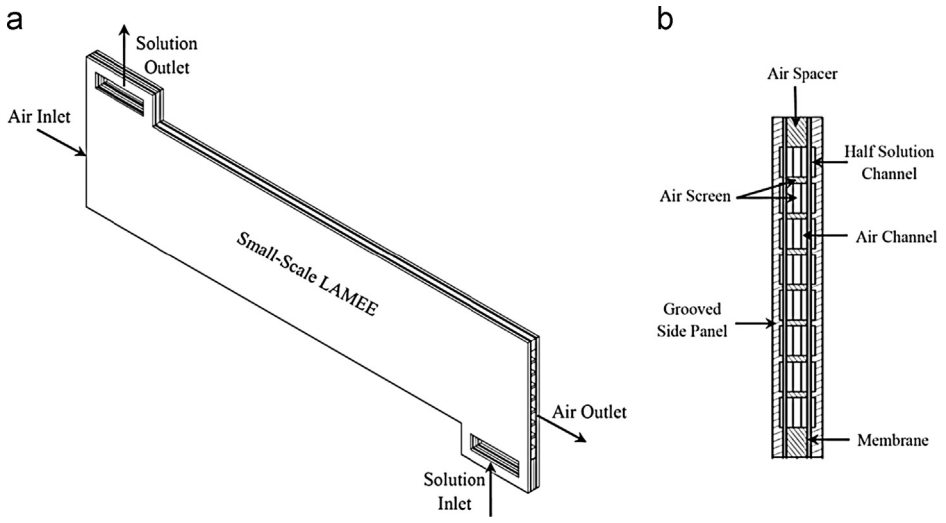

Fig. 17. (a) Flow configuration and (b) cross section view of the small-scale LAMEE [132].

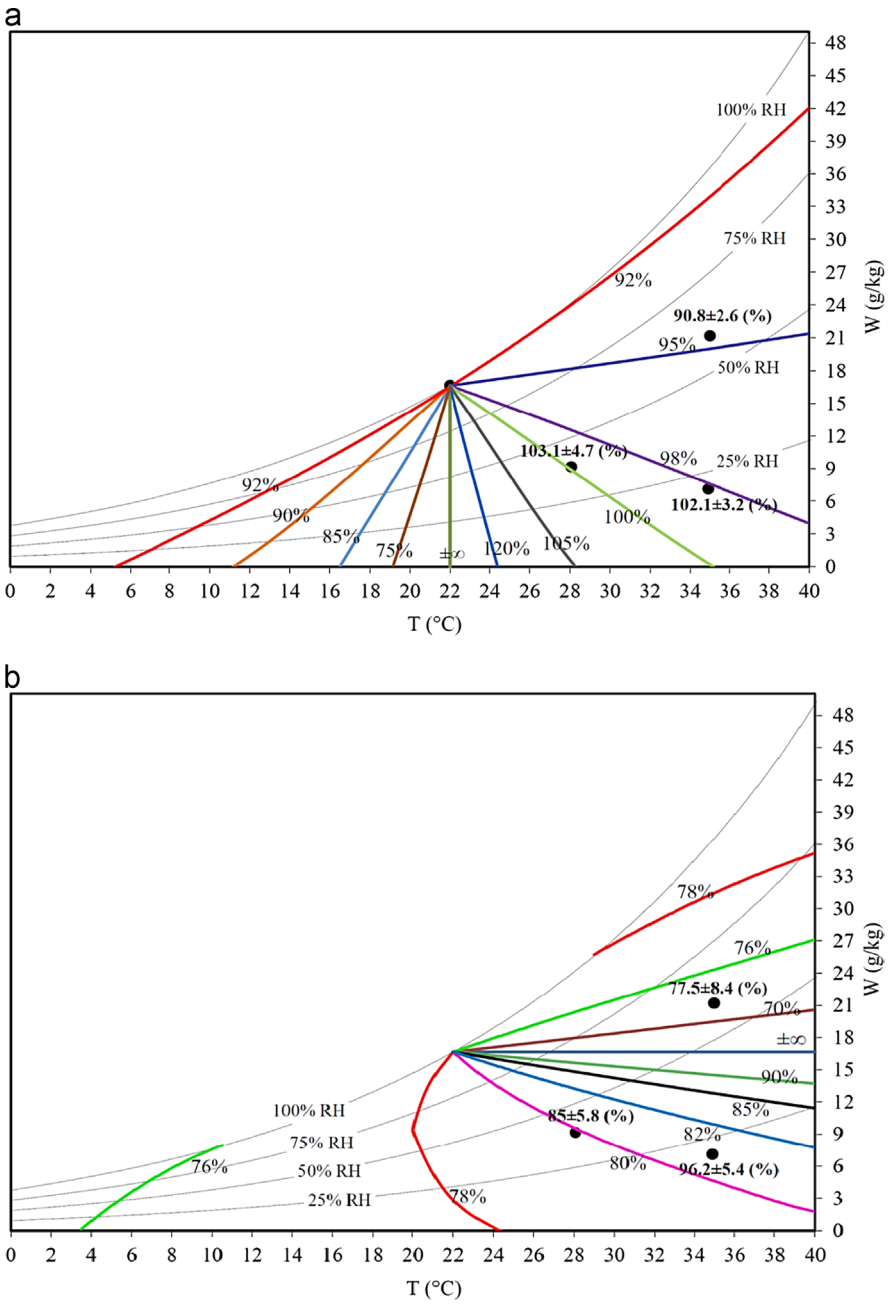

Fig. 18. Psychrometric chart with effectiveness values superimposed (a) sensible effectiveness, and (b) latent effectiveness contour maps for the small-scale LAMEE at $NTU=3.5$, $Cr^*=7$, $T_{sol,in}=22$ °C, and different inlet air conditions [132].

were in opposite directions (i.e. cooling and humidifying or heating and dehumidifying), the sensible effectiveness decreased as Cr^* increased. In all four processes, the latent and total effectivenesses increased as Cr^* increased. For the cooling and dehumidification process, Fig. 19 shows the air and desiccant solution inlet and outlet conditions for different types of desiccant solutions (i.e. LiCl and $MgCl_2$). It is obvious that type of desiccant solution did not has a significant effect on the LAMEE effectiveness, however, the total effectiveness increased by 10% when the concentration of the LiCl solution increased from 25% to 35%. Although the price of $MgCl_2$ is much lower than LiCl, Afshin et al. [140] recommended the use of LiCl in very dry climates to avoid any crystallization problems. Crystallization within the membrane pores will block water vapor transfer over part of each membrane surface area and result in lower latent and total effectiveness values. Due to the assumed coupling of phase change energy in the model, the simulation of sensible effectiveness will also not account for phase change energy when crystallization occurs.

NTU and Cr^* are considered the most important dimensionless numbers that affect LAMEE performance. Moghaddam et al. [138] studied the effect of *NTU* and Cr^* on the performance of the small-scale LAMEE for air cooling and dehumidifying under summer AHRI conditions [134]. Eight experiments were performed at *NTU* values of 4.5 and 5.8 and Cr^* values of 1, 3, 5, and 7. Results showed that the LAMEE effectivenesses increased as Cr^* or *NTU* increased, however Cr^* had a more significant influence on the effectivenesses compared to *NTU*.

When a hollow-fiber LAMEE was used for air humidification using water, Zhang and Huang [96] found that the airside resistance represented more than 98% of the total heat transfer resistance. This implies that the airflow channels in LAMEEs should be improved by convective heat transfer enhancement. Consequently, Moghaddam

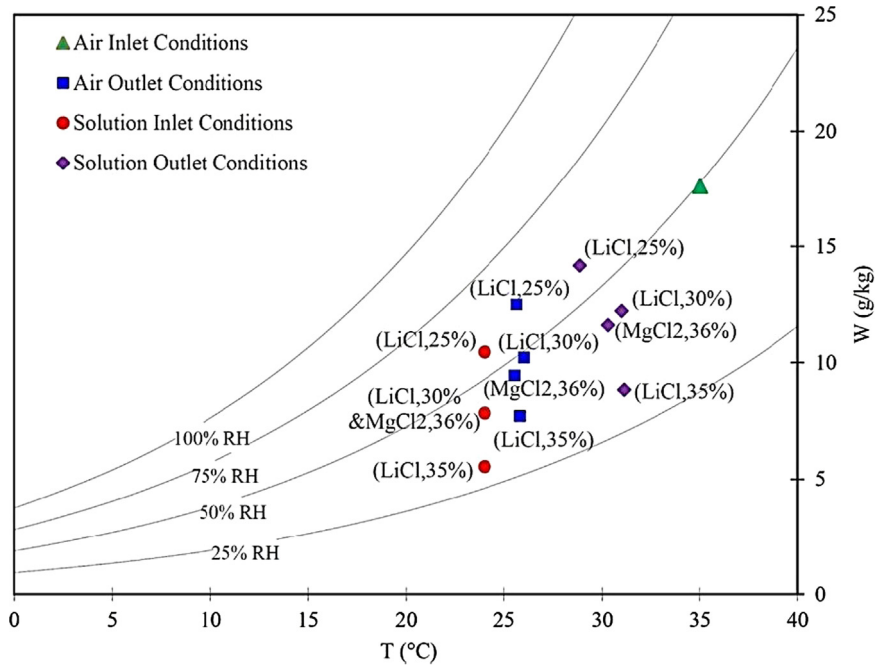

Fig. 19. Air and desiccant solution inlet and outlet conditions for different concentrations of LiCl and $MgCl_2$ during cooling and dehumidification experiments at $NTU=3$ and $Cr^*=5$ [137].

Table 4
Specifications of a counter-cross-flow LAMEE with gravity driven solution flow [144].

	Parameter	Value
Exchanger	Length (m)	1.06
	Height (m)	0.8
	Number of solution channels	10
	Maximum air flow capacity (cfm)	200
Membrane	Thickness (mm)	0.265
	Thermal conductivity (W/m K)	0.065
	Vapor diffusion resistance (s/m)	24

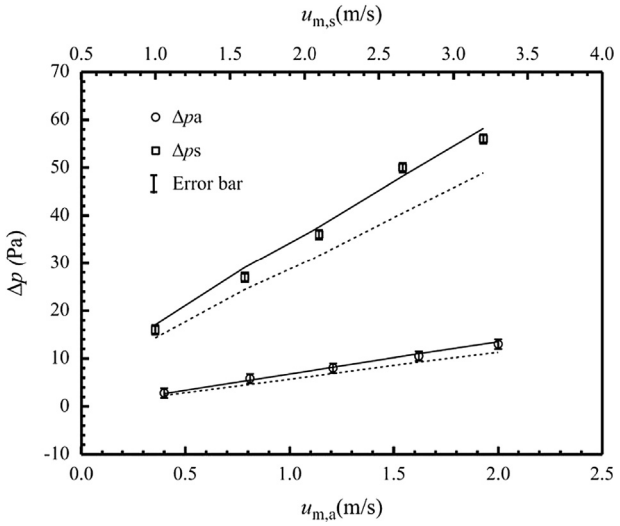

Fig. 20. Pressure drop across the LAMEE versus the flow velocity [current study experimental: discrete points, current numerical: solid lines, Huang et al. [146]: dotted lines] [147].

et al. [138] investigated the impact of using a turbulence enhancing insert in the air channel, on the effectiveness of the small-scale LAMEE. At $Cr^*=7$, the turbulence enhancing insert in the air channel enhanced the total effectiveness by 7% and 13% at *NTU* values of 5.8 and 4.5, respectively.

As mentioned before, a LAMEE can also be used to regenerate the diluted desiccant solution. Moghaddam et al. [139] experimentally studied the performance of the small-scale LAMEE as a regenerator. Fumo and Goswami [141] and Liu et al. [142] reported that during the regeneration process, providing the heat to the desiccant solution was more efficient than heating the air in counter-flow packed beds, therefore the LAMEE performance was evaluated under different desiccant solution inlet temperatures (i.e. 40, 45, 50, and 55 °C). The desiccant solution concentration, *NTU*, Cr^*, and the air inlet relative humidity and temperature were kept constant for all experiments. When the desiccant solution inlet temperature increased from 40 °C to 55 °C, the moisture removal rate increased by 450% whereas sensible, latent, and total effectivenesses decreased by 15%. These results revealed an important issue for selecting the optimum range for the desiccant solution inlet temperature in the regeneration process. If free thermal energy (e.g. waste heat or solar energy) is used to heat the desiccant solution, then higher desiccant solution temperatures would enhance the moisture removal rate. On the other hand, if the thermal energy must be purchased to heat the desiccant solution, then an economical study should be done to determine the best operating conditions. Further research is needed to determine the effect of other design and operating parameters (i.e. *NTU*, Cr^*) on the regenerator performance.

Semi-permeable membranes represent a significant part of a LAMEE's total initial cost, therefore using other less expensive materials as the contact surface between the air and desiccant solution can help to reduce the cost of a LAMEE. A LAMEE with a contact surface made of a special paper that allows simultaneous heat and moisture transfer between the air and desiccant solution, was employed as a dehumidifier in a liquid desiccant dehumidification system and its performance was experimentally studied by Jain et al. [143]. For their exchanger test models, the latent

effectiveness of their LAMEE varied between 25% and 44% and between 36% and 45% when $CaCl_2$ and LiCl were employed as the desiccant solutions, respectively. The concentration of the LiCl solution had no significant effect on the latent effectiveness of the dehumidifier. These latent effectiveness values were low compared to other LAMEEs that utilized a Polyethylene or Polypropylene semi-permeable membranes as the contact surfaces. Jain et al. [143] mentioned that the low latent effectiveness values were likely the consequence of (1) the non-uniform distribution of the desiccant solution inside this LAMEE, (2) the indirect contact between air and desiccant solution added more resistance for heat and mass transfer, and (3) the poor vapor permeability of the contact surface material used in their study.

Moghaddam et al. [144] experimentally and numerically studied the impact of outdoor air conditions on the performance of a counter-cross-flow LAMEE where the desiccant solution flowed through the LAMEE from top-to-bottom under the influence of gravity. This design may decrease the average pressure difference between the air and liquid channels and increase the membrane durability of the LAMEE used by Moghaddam et al. [144]. Table 4 gives the specifications of the studied LAMEE. The EPS code mentioned previously [94,121,124], was utilized to perform the numerical simulation. Results showed that under summer outdoor air conditions (35–39 °C and 16–22 g_v/kg_{air}), the sensible, latent, and total effectivenesses were 81%, 82%, and 82%, whereas they were 92%, 60%, and 78% under winter outdoor air conditions (0.3-1 °C and 0.5 g_v/kg_{air}). The substantial difference in the latent effectiveness between summer and winter operating conditions was thought to be due to the higher difference in relative humidity (i.e. higher mass transfer potential) between the air and liquid desiccant during the summer conditions [145]. The fact that the desiccant solution has water vapor removed for the winter test not only implies that there may be some potential for crystallization blockage of the membrane pores, but also the sensible effectiveness increases for the winter test relative to the summer test.

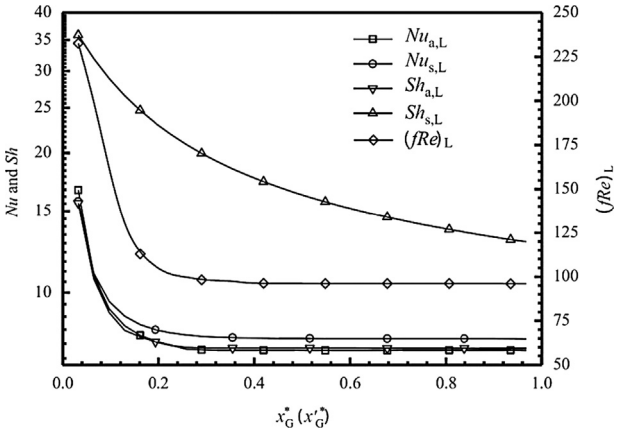

Fig. 21. Local (*fRe*), Nusselt and Sherwood numbers for air and solution streams versus Graetz number [147].

Huang et al. [146] developed a numerical model for a cross-flow LAMEE used for air dehumidification with LiCl solution. Results showed that after a short distance from the entry, the flow became thermally developed on both the air and solution sides. The local Sherwood number reached the minimum value quickly on the airside but was not able to reach it on the solution side, indicating the concentration boundary layer was not fully developed on the solution side. Consequently, for the solution side, the heat transfer was fully developed after a short distance from the entrance whereas the mass transfer was not fully developed at the exit and thus the solution stream had a much higher Sherwood number than the air stream.

The pressure drop through a LAMEE and the noise level are affected by the exchanger length, therefore the exchanger length

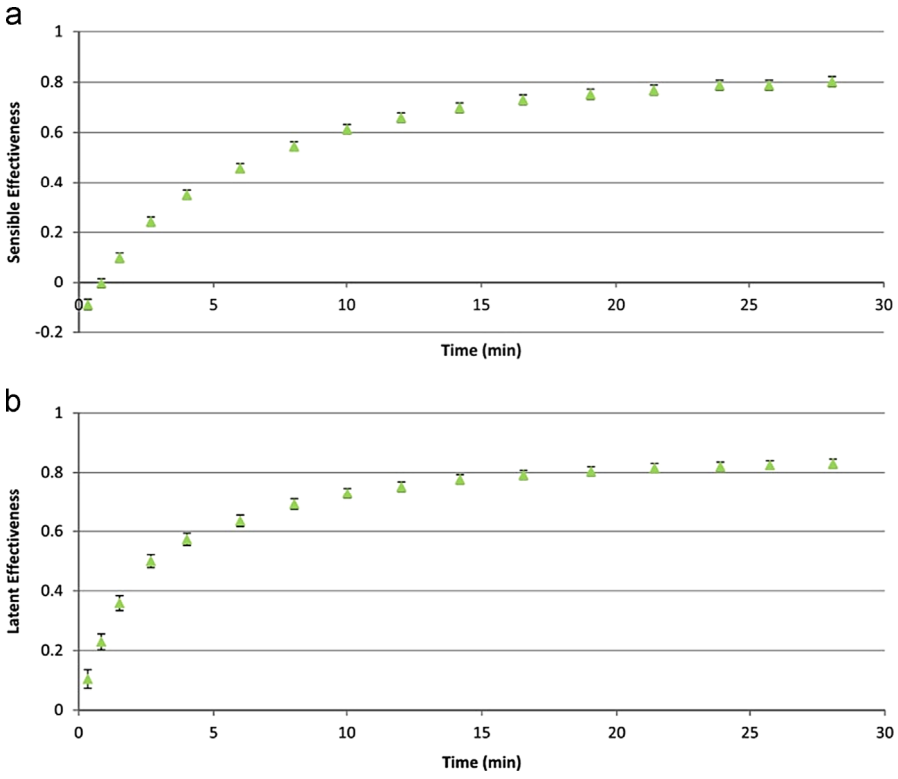

Fig. 22. Transient (a) sensible effectiveness and (b) latent effectiveness versus time under summer operating conditions at $NTU=8$, $Cr^*=6.3$, $T_{air,in}=34$ °C, and $W_{air,in}=25.6$ g_v/kg_{air} [126].

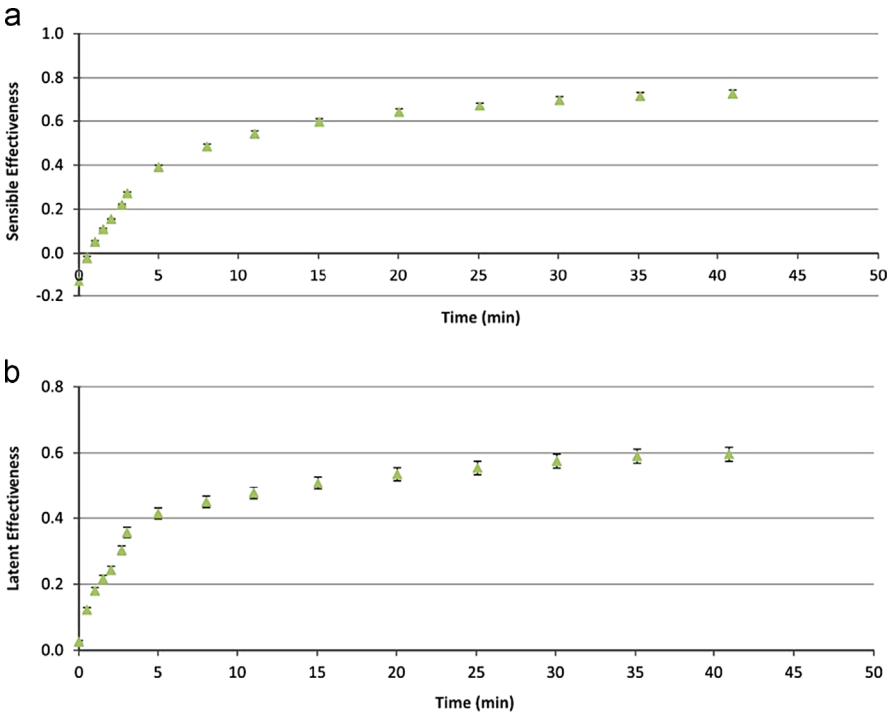

Fig. 23. Transient (a) sensible effectiveness and (b) latent effectiveness versus time under winter operating conditions at $NTU=8$, $Cr^*=3$, $T_{air,in}=7.8$ °C, and $W_{air,in}=3.1$ g_v/kg_{air} [126].

should be kept as short as possible [147]. Huang et al. [146] studied the conjugate heat and mass transfer in a LAMEE for air dehumidification with developing heat and mass transfer, where a fully developed flow was assumed. However the assumption of fully developed flow was found to be inaccurate. Huang et al. [147] studied the effect of the developing entrance lengths on the fluid flow and the conjugate heat and mass transfers in a cross-flow LAMEE. Fig. 20 shows that the pressure drop in the air and solution channels increases as the flow velocity increases and the experimental results agreed quite well with the numerical results. Fig. 21 shows that the fluid flow and heat and mass transfer became fully developed after 30% of the channel length for the airside. For the solution side, the fluid flow and heat transfer became fully developed after 30% of the channel length but the mass transfer did not become fully developed inside the channel. A comparison with Huang et al. [146] confirmed that assuming either the hydrodynamic, thermal, or concentration boundary layers are fully developed caused underestimations in the results.

8.1.2. *Transient performance*

The transient response of a flat-plate LAMEE is a crucial issue both during the system start-up and when the outdoor air conditions experience rapid fluctuations. Namvar et al. [126] experimentally investigated the transient performance of a counter-cross-flow LAMEE. The LAMEE specifications are given in Table 2. The transient performance of a LAMEE can be characterized using a time constant which is the time required by the transient outlet variable to reach 63.2% of the difference between its initial and final values [126]. Data showed that the temperature time constant response delay was longer than the humidity ratio time constant, i.e. the steady-state condition was attained in the case of latent heat transfer faster than the sensible heat transfer likely because the thermal mass of the exchanger was significant. Steady-state was achieved in less than 1 h at all mass flow rates. Figs. 22 and 23 show that during summer operating conditions, the sensible and latent effectivenesses increase with time with a similar trend and had a value higher than 80% after 27 minutes whereas during winter conditions, the sensible and latent effectivenesses reached 75% and 60%; respectively, after 42 minutes. The sensible effectiveness is negative at the beginning of the test when the desiccant solution inside the LAMEE is in thermal equilibrium with the air, due to the release of phase change energy during dehumidification which causes the air outlet temperature to be higher than the air inlet temperature.

Namvar et al. [127] also numerically investigated the transient response of the counter-cross-flow LAMEE and used Namvar et al. [126] experimental results to validate the numerical model. The average absolute difference was calculated to evaluate the agreement between the experimental and numerical results. The difference was less than 0.1 for sensible effectiveness whereas it was less than 0.05 for latent and total effectivenesses. Fig. 24 shows that at a constant Cr^*, the transient time constant increases as NTU increases. There is good agreement between the experimental and numerical results for the LAMEE's latent response but poor agreement for the LAMEE's thermal response. Fig. 25 shows that outdoor air conditions have a negligible effect on the sensible time constant whereas they have a significant effect on the latent time constant (i.e. mass transfer response), the latent time constant decreased as H^* increased. It can be concluded that the response time delay mainly depends on Cr^* and NTU; the response time decreases as Cr^* increases and increases as NTU increases.

As shown in Figs. 22 and 23, the sensible and latent effectivenesses were higher during summer operating conditions than during winter operating conditions. Fig. 26 shows that during winter operating conditions, the Richardson number was higher than 10 and thus there was significant natural convection between the hot liquid desiccant and the cold membrane [127,148]. Richardson number gives an indication about the ratio between the potential and kinetic energies. Grashof number is the ratio between the buoyancy and viscous forces. Yao [149] reported that if the Grashof number is less than the Reynolds number, buoyancy effects can be neglected in isothermal vertical channels. Fig. 26 shows that the Grashof number was 2–12 whereas Reynolds number was <1 and thus buoyancy forces had a considerable

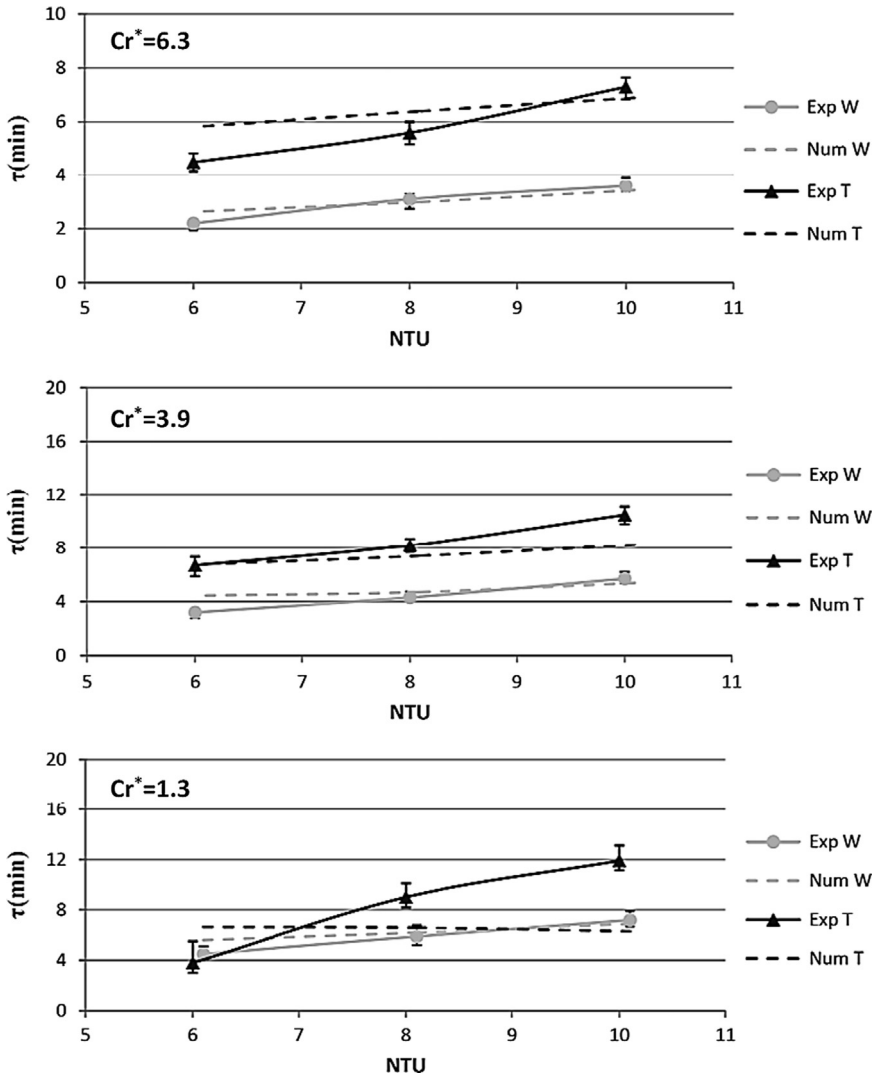

Fig. 24. Comparison between numerical and experimental time constants at different *Cr** under summer operating conditions [127].

adverse effect on LAMEE performance under winter operating conditions [127].

8.2. The hollow-fiber LAMEE

Research on hollow-fiber LAMEEs started in 2000 at the University of Genoa when Bergero and Chiari [150] carried out theoretical and experimental work to investigate heat and moisture transfer inside a hollow-fiber LAMEE during air humidification and dehumidification processes. LiCl solution and water were employed as the working fluids for air dehumidification and humidification, respectively. Bergero and Chiari [150] built a hollow-fiber LAMEE prototype at the University of Genoa in Italy. The structure and dimensions of the prototype are shown in Fig. 27. It was composed of 800 polypropylene hollow fibers assembled together in a rectangular geometry. The polypropylene hollow fibers were arranged in a staggered configuration with an average void fraction of 0.4–0.45, a total fiber external surface area of 1.2 m^2, and heat/mass transfer area per unit volume of 593 m^2/m^3. Each hollow fiber has an outer diameter of 1 mm, a wall thickness of 0.2 mm, and a mean membrane pore radius of 0.2 μm. The air flowed in a direction normal to the polypropylene hollow fibers while the LiCl solution flowed through the hollow fibers. A theoretical model was developed using a finite volume technique and experimental results agreed with the theoretical results. Table 5 shows the pressure drop on the air and water sides. Generally, the latent effectiveness decreased as the air flow rate increased whereas the LiCl solution and water flow rates did not have a significant effect on the effectiveness.

Air humidification using water was investigated by Chiari [151] using the test facility presented in Bergero and Chiari [150]. The air inlet temperature and relative humidity were 24 °C and 50% RH, respectively, and the water inlet temperature was 19 °C. A higher latent effectiveness was achieved at higher water flow rates whereas the latent effectiveness decreased as the air flow rate increased. At a constant air inlet temperature, the latent effectiveness increased as the water inlet temperature decreased, or as the membrane thickness decreased. An effectiveness of 90% was achieved with a hollow fiber wall thickness of 50 μm at water and air inlet temperatures of 10 °C and 15 °C, respectively.

Zhang and Huang [96] developed a theoretical model and conducted experimental work to investigate the performance of a counter-flow hollow-fiber LAMEE for air humidification using water. The experimental setup is shown in Fig. 28. Fig. 29 shows that when *NTU* increased, the latent effectiveness significantly increased and the average moisture permeability (*Pe*) decreased. Fig. 30a shows that increasing either the water or the air mass flow rate increased the pressure drop. A much higher increase in the pressure drop occurred as the water mass flow rate increased, compared to the air mass flow rate. The effects of the water and air mass flow rates on the sensible

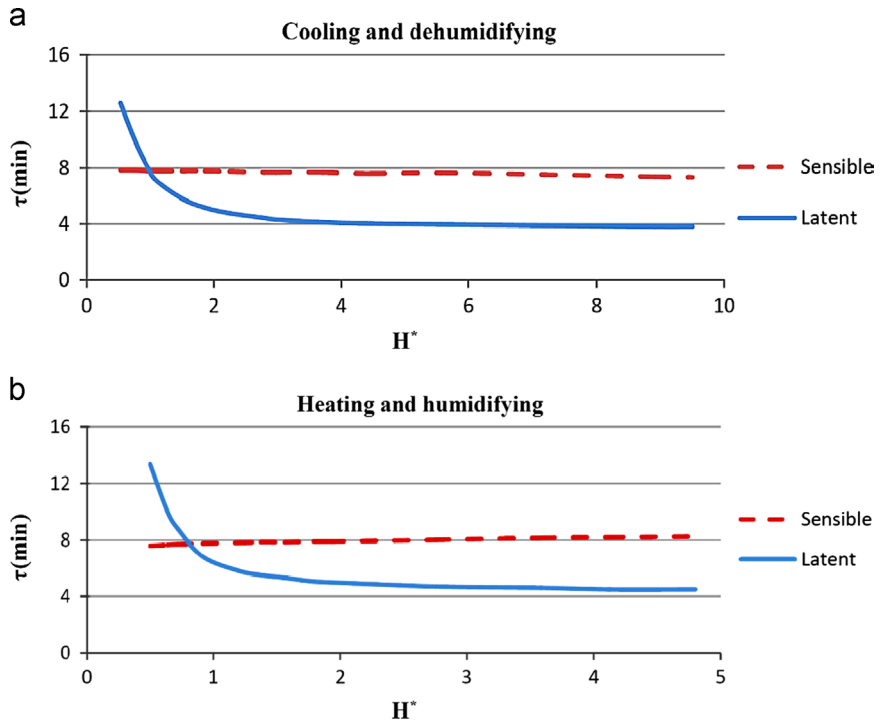

Fig. 25. Sensible and latent time constants versus H^* for (a) cooling & dehumidification and (b) heating & humidifying at $NTU=8$, $Cr^*=6.3$, $T_{sol,in}=24\ ^\circ C$, and $W_{sol,in}=9.3$ g/kg [127].

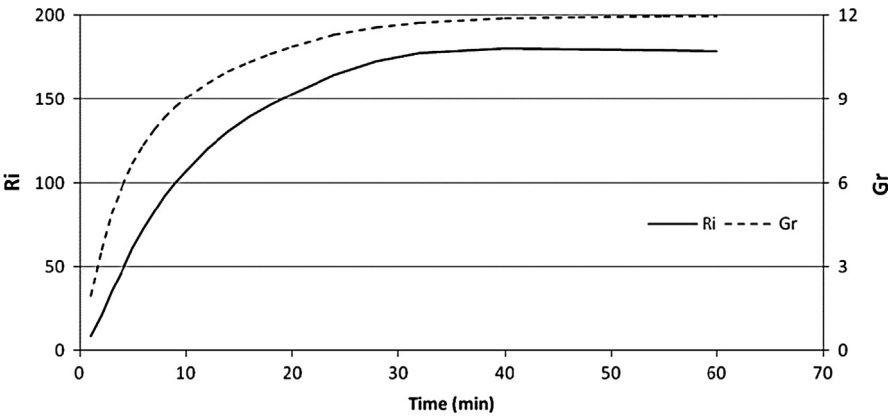

Fig. 26. Grashof and Richardson numbers versus time under winter operating conditions [127].

and latent effectivenesses are compared in Fig. 30b. Neither the water or air mass flow rates had a significant effect on the sensible effectiveness but the latent effectiveness decreased significantly when the air mass flow rate increased. Table 6 shows that more than 98% of the total heat transfer resistance is attributed to the airside whereas the membrane accounts for 84% of the total mass transfer resistance. Therefore, moisture transfer could be enhanced by improving the membrane properties whereas the airside convective resistance is the key for heat transfer enhancement.

The packing fraction gives an indication of the volume occupied by the hollow fibers inside the LAMEE and has a significant influence on the effectiveness and pressure drop of a hollow-fiber LAMEE. Zhang and Huang [96] studied the impact of the packing fraction on the performance of a counter-flow hollow-fiber LAMEE. It is shown in Fig. 31a that increasing the packing fraction did not have a significant effect on the total mass transfer coefficient. Fig. 31b shows that increasing the packing fraction causes a significant increase in the latent effectiveness and in the pressure drop on the shell side, a slight decrease in the pressure drop on the fibers side, and almost no effect on the sensible effectiveness. The enhancement in the latent effectiveness was due to the increase in the contact surface area not the transfer coefficients.

Zhang [89] developed an analytical model for a counter-flow hollow-fiber LAMEE and performed experimental work to validate this analytical model. Fig. 32 shows the experimental facility. The desiccant solution was pumped through a dehumidifier where the fresh air was cooled and dehumidified, causing the desiccant solution to became diluted. The diluted desiccant solution was heated in a hot water bath and then it flowed through a regenerator to increase the desiccant concentration. Finally, the regenerated desiccant solution flowed through a cold water bath and then back to the dehumidifier. Fig. 33 shows that at low air mass flow rates, the sensible effectiveness was higher than the latent effectiveness and both effectivenesses decreased with an increase in the air mass flow rate. The parameters that had the most significant influence on the effectivenesses were NTU and NTU_m.

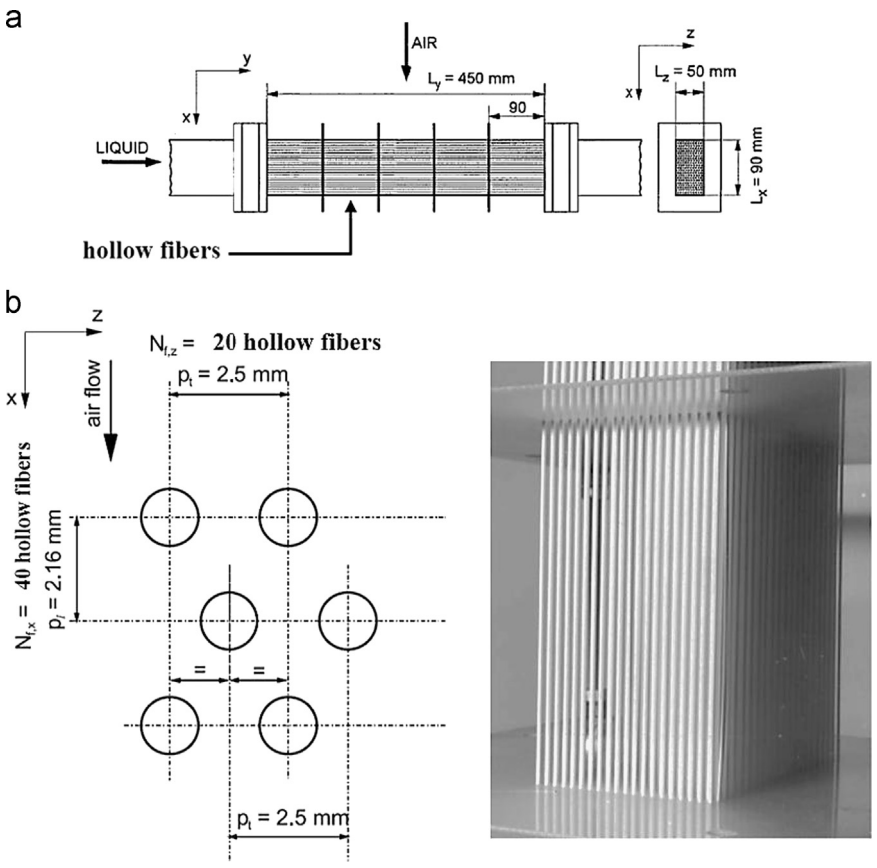

Fig. 27. Structure and dimensions of the hollow-fiber LAMEE prototype built at the University of Genoa [150].

Table 5
Pressure drop in the hollow-fiber LAMEE [150].

Fluid	Pressure drop (Pa)	Flow rates
Air	30–70	30–80 (m^3/h)
Water	1310–3350	19–54 (kg/h)

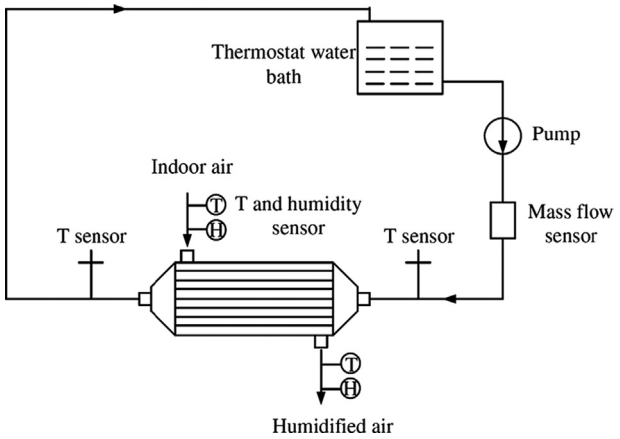

Fig. 28. The experimental setup used for air humidification using water [96].

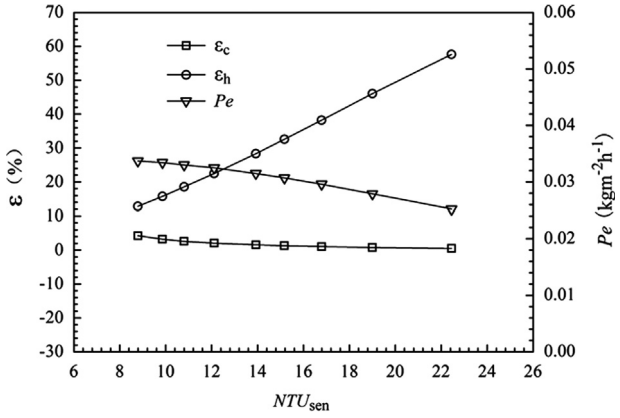

Fig. 29. Effect of *NTU* on sensible and latent effectivenesses and average permeability [96].

The hollow fibers can either be packed regularly or randomly inside the hollow-fiber LAMEE. Zhang [152] developed a theoretical model to investigate the effect of random distribution of the hollow fibers on the heat and mass transfer processes during air humidification using water. Fig. 34 shows a photograph of the hollow fibers packed inside the LAMEE. Results showed that as the packing fraction increased, the packing became more regular. At a packing fraction of 0.2–0.6, which is common for most hollow-fiber LAMEEs, the Sherwood number with random packing was around 1–5% of that for the regular packing, which means that there was a significant deterioration in the performance of the hollow-fiber LAMEE when randomly packing was used. This is because when the hollow fibers are randomly packed, more fluid flows through the large pinholes (volume between hollow fibers), which causes a reduction in the active membrane surface area available for solution and air contact.

After determining that increasing the packing fraction in a counter-flow hollow-fiber LAMEE with a cylindrical shell caused a significant increase in the pressure drop on the shell side [96], Zhang [95] investigated, experimentally and theoretically, the performance of a cross-flow hollow-fiber LAMEE with a

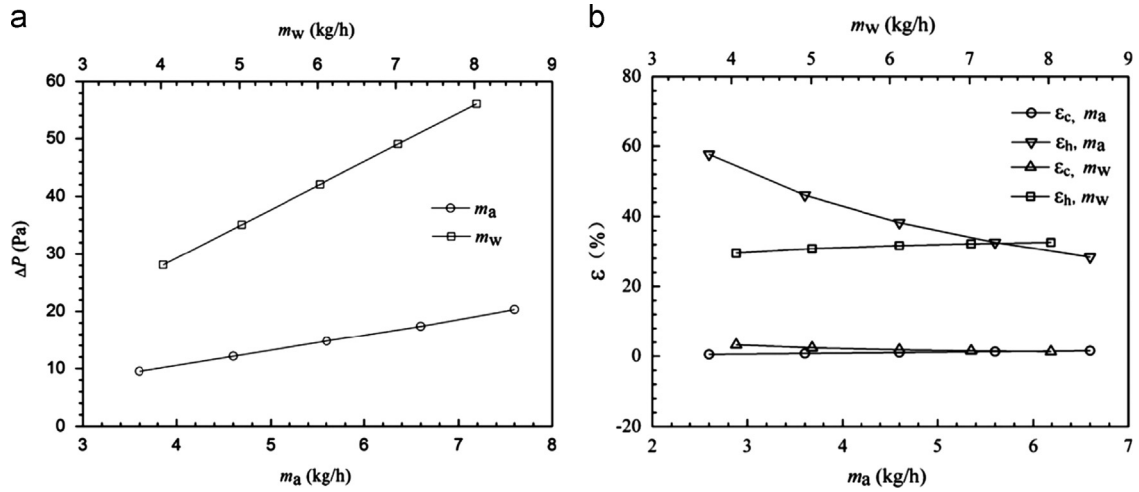

Fig. 30. Effect of water and air mass flow rates on (a) pressure drop and (b) sensible and latent effectivenesses (m_{air} is kept at 5.6 kg/h when m_w is varied and m_w is kept at 8.03 kg/h when m_{air} is varied) [96].

Table 6
Resistance for heat and mass transfer in the hollow-fiber LAMEE [96].

Resistance	Heat transfer resistance Percentage (%)	Mass transfer resistance Percentage (%)
Liquid side	1	0
Membrane		
Support layer	0.0001	74
Skin layer	0.0002	10
Total	0.002	84
Air side	99	16
Total	100	100

rectangular shell used for air humidification with water. A prototype of the hollow-fiber LAMEE with a rectangular shell, shown in Fig. 35, was built. The prototype was composed of 2900 hollow fibers packed inside a rectangular shell where water flowed through the hollow fibers and air flowed across them. Table 7 shows that when the packing density increased from 0.19 to 0.59 (i.e. 2000 to 6000 fibers), the pressure drop decreased on the tube side and increased on the shell side. *NTU* and NTU_m increased by 383% and 211%, respectively, for this change in the packing density however the increase in *NTU* was higher and thus the Lewis number (Le_{tot}) increased. There was no change in the resistance to heat and moisture transfer of the membrane, whereas the airside resistances decreased as the packing density increased. Compared to an aligned arrangement, the airside pressure drop and convective heat and moisture transfer coefficients for a staggered arrangement increased by 335%, 11% and 5%, respectively. Consequently, in contradiction to the traditional sensible shell and tube exchanger, the packing density had a more significant effect on the performance than the array arrangement in the hollow-fiber LAMEE. In conclusion, a high packing density with an aligned arrangement was recommended for higher effectiveness and lower pressure drop.

Zhang et al. [90] developed a numerical model to investigate the conjugate heat and mass transfer in a cross-flow hollow-fiber LAMEE for air dehumidification using LiCl solution. Due to the difficulty in simulating the whole module, the study was performed on a single hollow fiber where the LiCl solution flowed through the fiber and the air flowed across the fiber. Fig. 36 shows a schematic of the hollow fiber used in the numerical model, where β is the angle of the air contact point with the hollow fiber. It is shown in Fig. 37 that at higher Reynolds numbers, the Nusselt and Sherwood numbers of the air were maximums at the front stagnation point (i.e. $\beta=0$) and decreased as β increased. The

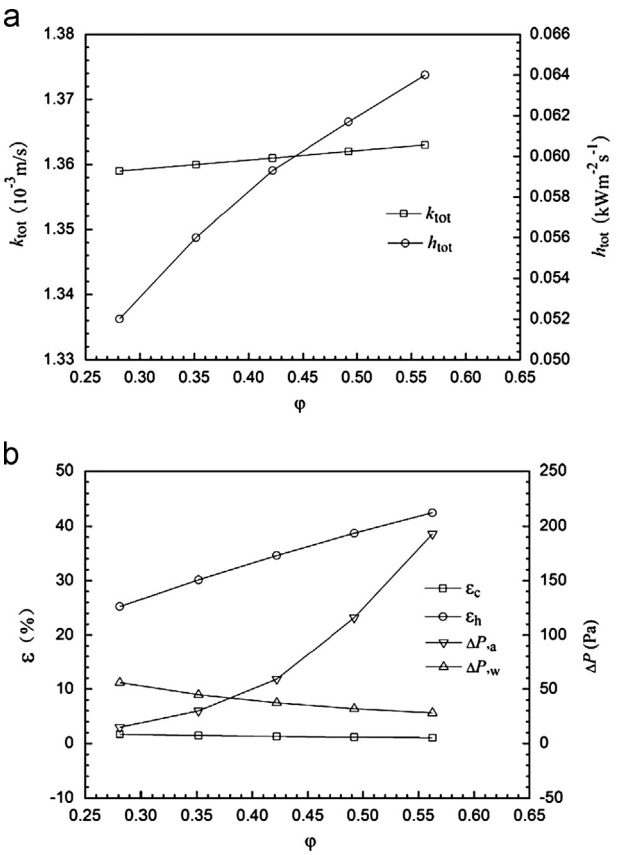

Fig. 31. Influences of packing fraction on (a) total heat and mass transfer coefficients and (b) the sensible and latent effectivenesses, and fiber side and shell side pressure drops [96].

Nusselt and Sherwood numbers started increasing again at $\beta=150$ due to the higher turbulence in the rear region of the fiber.

Zhang et al. [90] compared the performance of this cross-flow [90] and a counter-flow [91] hollow-fiber LAMEE. The counter-flow hollow-fiber LAMEE was studied by Zhang et al. [91]. Fig. 38 shows a comparison between the overall average Nusselt and Sherwood numbers and the pressure drop on the airside for the cross-flow and the counter-flow hollow-fiber LAMEEs. At Reynolds number lower than 35, the counter-flow configuration had higher Nusselt and Sherwood numbers. At Reynolds numbers higher than 35, the Nusselt and Sherwood numbers of the cross-flow configuration were

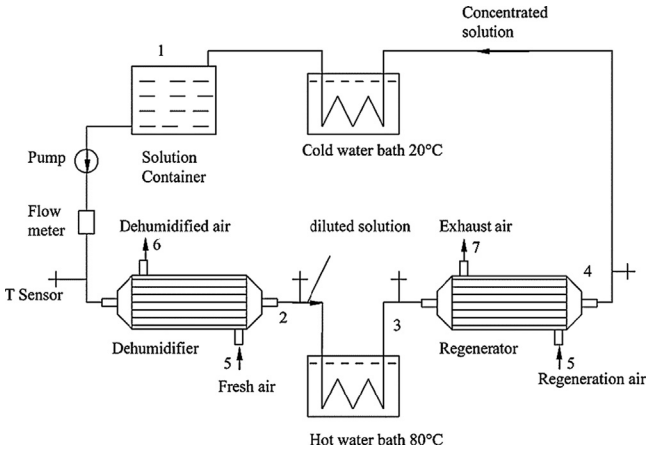

Fig. 32. The experimental facility used to test a counter-flow hollow-fiber LAMEE [89].

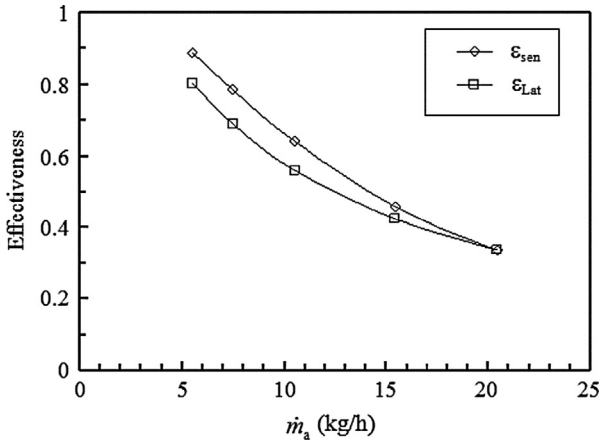

Fig. 33. Sensible and latent effectivenesses versus mass flow rate of air [89].

Fig. 34. Photograph of the hollow fibers inside the hollow-fiber LAMEE [152].

much higher than that of the counter-flow configuration due to the vortexes behind the fibers [153–155]. The airside pressure drop in the cross-flow LAMEE was lower than that in the counter-flow LAMEE. Consequently, the cross-flow configuration is more attractive for applications than the counter-flow configuration.

Laminar flow was assumed in [90] as the Reynolds number of the air flow was low (200–600), however, the large number of fibers (3000–12,000) caused a continuous disturbance of the air

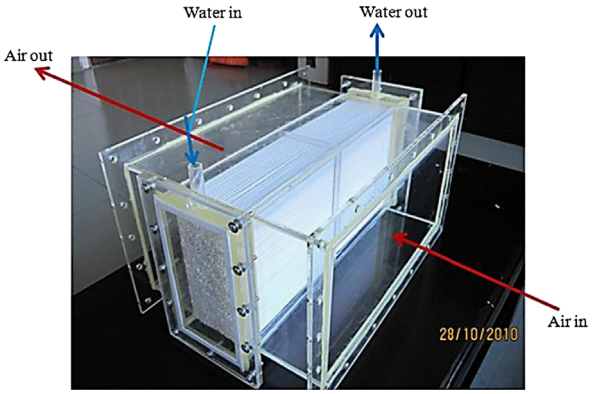

Fig. 35. The hollow-fiber LAMEE prototype with a rectangular shell [95].

Table 7
Influences of packing density on performance of the rectangular hollow-fiber LAMEE [95].

Parameters	Number of fibers packed (n_{fr})				
	2000	3000	4000	5000	6000
ε_{sen}	1.3	1.35	1.36	1.36	1.35
ε_{Lat}	0.5	0.58	0.62	0.65	0.67
$\dot{m}_{rr}$ (g_w/h)	574	662.5	710.8	740.6	761
NTU	6.5	10.8	15.9	22.4	31.4
NTU_m	0.9	1.4	1.8	2.3	2.8
ΔP_{air} (Pa)	2.2	4.5	9	19.7	52.8
ΔP_w (Pa)	29.6	19.7	14.8	11.8	9.9

flow and thus the air flow became turbulent [156]. Consequently, Huang et al. [157] developed a theoretical model to investigate the conjugate heat and mass transfer in a cross-flow hollow-fiber LAMEE for air dehumidification with turbulent flow. The local turbulent Reynolds numbers were less than 150 and thus the standard $k-\varepsilon$ turbulence model was not efficient to model the flow near the wall [158,159]. Instead, a low Re $k-\varepsilon$ model [158,159] was used to study the air flow. The results showed that the values of the mean Sherwood numbers were quite close to the Nusselt numbers and both numbers increased as the packing fraction increased. For the fiber side, the fully developed Sherwood numbers were higher than the fully developed Nusselt numbers.

Research on the hollow-fiber LAMEE with turbulent flow was continued when Zhang and Li [160] investigated the convective mass transfer and pressure drop on the bundle side in the hollow-fiber LAMEE at low Reynolds number but unstable transitional flow. Results revealed that the convective mass transfer increased as Reynolds number increased and the impact of the transverse pitch on the mass transfer and pressure drop is stronger than that of the longitudinal pitch. Zhang and Li [160] developed correlations to calculate the mean Sherwood number and the friction factor for the hollow-fiber LAMEEs. They used the *Chilton–Colburn analogy* to obtain Sherwood numbers from different work available in the literature. However, Zhang [161] reported that the *Chilton–Colburn analogy* may not be applicable for membrane energy exchangers if there is a big difference between dimensionless boundary conditions for heat and mass transfer. As shown in Table 8, they found a good agreement between the correlations and results reported in the literature.

$$Sh_m = C\mathrm{Re}^m Sc^{0.333} \tag{17}$$

$$f = a\mathrm{Re}^b \tag{18}$$

where Sh_m is the mean Sherwood number, Re is Reynolds number, Sc is Schmidt number, f is the friction factor, C, m, a, and b are constants [160].

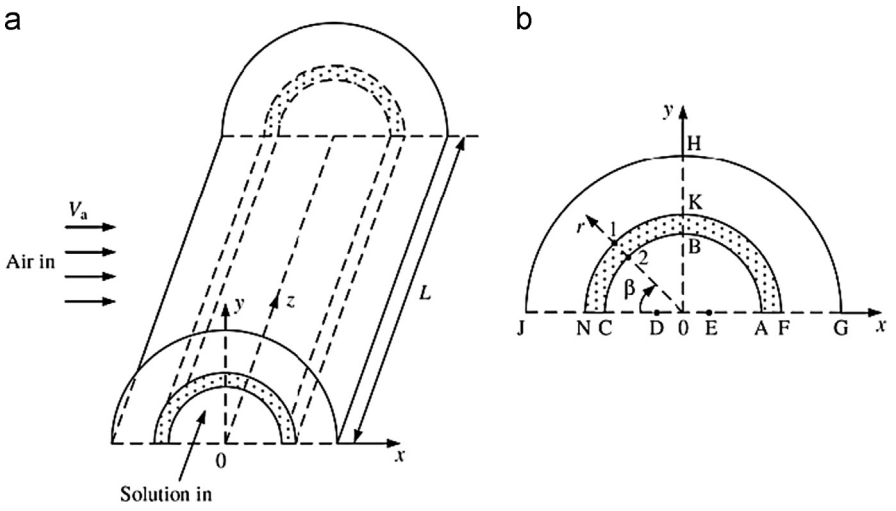

Fig. 36. (a) The three dimensional coordinates system of a single hollow fiber and (b) the physical system [90].

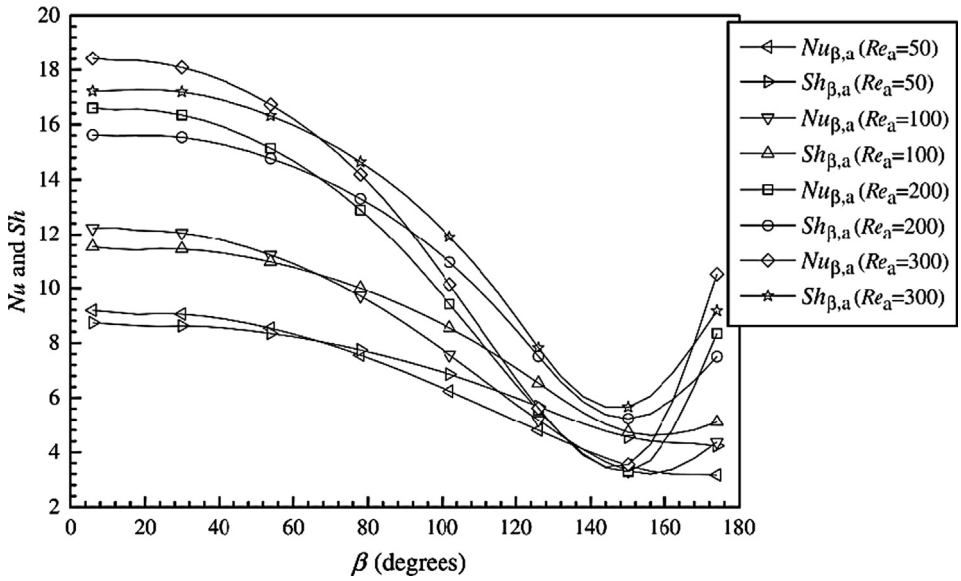

Fig. 37. Nusselt and Sherwood numbers for the air flow versus angular position on the fiber at different Reynolds numbers (ϕ=0.265) [90].

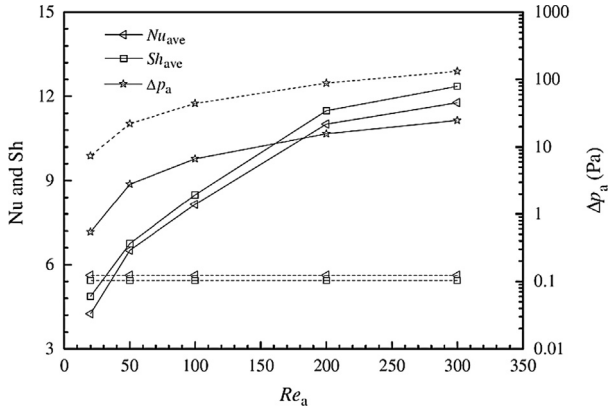

Fig. 38. Comparison between the average Nusselt and Sherwood numbers and pressure drop on the air side for the cross-flow (solid lines) and counter-flow (dotted lines) [91] configurations at packing fraction of 0.265 [90].

Table 8
Sherwood number from the proposed correlations and literature (S_T=S_L=1.5d) [160].

Re	Zhang and Li [160]	Grimison [162]	Zukauskas [163]	Hausen [164]	Khan et al. [165]
Inline					
100	6.61	7.88	7.25	6.87	11.84
200	10.63	12.11	10.25	11.11	16.74
300	14.03	15.57	12.55	14.57	20.51
400	17.08	18.61	14.49	17.59	23.68
500	19.90	21.37	16.20	20.33	26.48
Staggered					
100	10.23	10.41	9.89	10.18	14.91
200	15.13	15.37	13.99	15.11	21.08
300	19.01	19.30	17.14	19.04	25.82
400	22.36	22.69	19.79	22.44	29.81
500	25.36	25.72	22.12	25.48	33.33

8.3. *The three-fluid LAMEE*

During air humidification and dehumidification processes, heat of phase change is absorbed from/released to the desiccant solution flow and thus the temperature of the desiccant solution changes inside a LAMEE. Consequently, the potential for heat and moisture transfer deteriorates across the length of a LAMEE. The impact of the heat of phase change can be eliminated by using a

refrigerant or water to keep the temperature of the desiccant solution constant in the exchanger. In direct-contact liquid desiccant systems, internally cooled dehumidifiers/heated regenerators have been suggested and studied by several scholars [166-176]. Currently, the authors of this review paper are working on the development and research of an innovative three-fluid flat-plate LAMEE at the University of Saskatchewan.

Isetti et al. [177] presented an innovative three-fluid LAMEE where water was employed to control the desiccant solution temperature. They used a commercial aluminum evaporator (225 mm × 190 mm × 58 mm) to manufacture a prototype for the three-fluid LAMEE at the University of Genoa. The evaporator was modified where hydrophobic micro-porous polypropylene hollow fibers replaced the finned surfaces between the cooling plates. As shown in Fig. 39, the refrigerant flowed through the cooling plates and controlled the temperature of the desiccant solution flowing around the hollow fiber membranes. For the first time in a LAMEE, Potassium Formate (KCOOH) was employed as the liquid desiccant for air dehumidification; KCOOH is thermally stable, non-flammable, and exhibits excellent thermophysical properties [178]. Water was used for air humidification. A theoretical model was developed and the results agreed well with the experimental results. The total effectiveness of the prototype was around 25% during experiments. Consequently, a theoretical sensitivity study was performed to determine the effect of various operating and design parameters on the total effectiveness. A total effectiveness higher than 95% was predicted by manipulating the number and thickness of the hollow fiber membranes and the temperature of the cooling water. Based on these promising results, a new prototype is being designed and under construction at the University of Genoa.

9. Flow maldistribution in LAMEEs

Flow maldistribution deteriorates thermal performance of heat exchangers and increases the pressure drop as well [179,180]. Mueller and Chiou [181] presented a comprehensive review on different types of flow maldistribution and how it affects the performance of heat exchangers. Flow maldistribution may occur

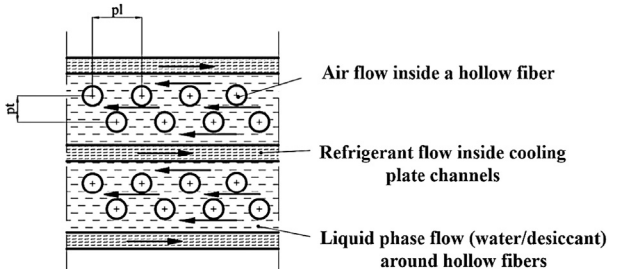

Fig. 39. Flow configuration of the three fluids inside the three-fluid LAMEE [177].

because of (1) poor exchanger design (e.g. uneven channel thicknesses), (2) heat transfer processes (e.g. frosting, vibration patterns resulting from physical flow), (3) operation of external systems (e.g. pumps, fans) [182], or (4) fouling and corrosion problems [181].

Lalot et al. [183] found that flow maldistribution deteriorated the thermal performance of a cross-flow heat exchanger by more than 25%. It was noted in [179] that for a heat pump unit, Elgowainy [184] reported that as a result of increased pressure drop, flow maldistribution may deteriorate the hydraulic performance by 6–9 times as much as thermal performance. T'joen et al. [185] found that non-uniform flow profiles decreased the overall heat transfer coefficient of a fin-and-tube heat exchanger by 8%. Performance deterioration of heat exchangers caused by flow maldistribution strongly depends on *NTU*. Performance deterioration is less than 5% at low *NTUs* ($NTU < 4$) but increases at $NTU > 10$ [181]. Moreover, deterioration in exchanger performance for laminar flow is more significant than that for turbulent flow. In general, flow maldistribution reduces the performance of heat exchangers by 5–15% [182].

In air-to-air membrane energy exchangers, Zhang [35] found that deterioration in thermal and latent performances of a plate-fin membrane energy exchanger due to flow maldistribution can be neglected for a channel pitch smaller than 2 mm, but when the channel pitch was larger than 2 mm, thermal and latent performances reduced by 10–15% and 20–25%, respectively. Zhang [38] reported that maldistribution reduced the thermal and latent performances of a flat-plate membrane energy exchanger by less than 9% for a channel pitch smaller than 2 mm, and 28% for a channel pitch larger than 2 mm.

9.1. Flow maldistribution in flat-plate LAMEEs

Flow maldistribution may occur in a flat-plate LAMEE due to the causes mentioned previously, however, the majority of flow maldistribution may occur due to deflection of the membrane. The large pressure difference between the solution and air channels across the membrane under normal operation conditions, causes the membrane to deflect into the air channels and thus the air channels may become partially or fully blocked. The degree of the membrane deflection mainly depends on the magnitude of the pressure difference across the membrane, the membrane's modulus of elasticity, the membrane's surface area, solution and air channel thicknesses, and the ratio between solution and air mass flow rates (Cr^*).

In 2005, Hemingson [128] tested a cross-flow LAMEE prototype where the air channels were partially blocked at high operating pressures which significantly deteriorated the LAMEE effectiveness. Support grids with different geometries were proposed to support the membrane. The grids exhibited a good support for the

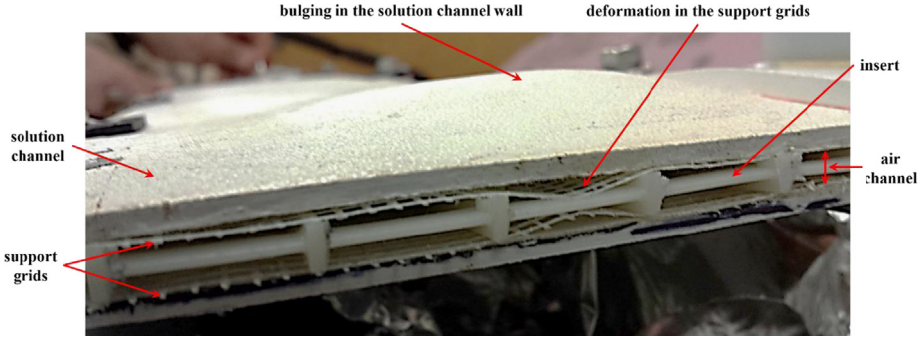

Fig. 40. Photograph of deformations that occurred in a flat-plate LAMEE tested at the University of Saskatchewan.

membrane and contributed, somewhat, to solve the maldistribution problem, however maldistribution was not completely eliminated.

Fig. 40 shows a photograph of the deformations that occurred in a flat-plate LAMEE prototype tested at the University of Saskatchewan. It is clear that the support grids are deformed into the air channel due to the pressure difference between the solution and air sides. The membrane deflection decreases the cross-sectional area of the air channels, which results in a higher air velocity and thus an increase in the convective heat transfer, but also results in a decrease in the amount of air contacting the membrane, and an increase in the pressure drop on the airside.

Studying the impact of the flow maldistribution on the effectiveness of the flat-plate LAMEE is difficult due to (1) difficulty of operating a LAMEE without any maldistribution as a benchmark, (2) difficulty of controlling the amount of maldistribution for different testing conditions, and (3) difficulty of getting accurate measurements for membrane deflections during the operating process. No work on flow maldistribution in flat-plate LAMEEs has been reported in the literature and thus the influences of maldistribution on the performance of a flat-plate LAMEE are not fully identified and still an important issue.

9.2. Flow maldistribution in hollow-fiber LAMEEs

In addition to the reasons discussed previously, flow maldistribution may occur in hollow-fiber LAMEEs due to the movement or vibration of the fibers. The flow of the air can cause movement of the hollow fibers and they may come in contact with each other at high air pressures, therefore decreasing the heat and mass transfer surface area. The degree of maldistribution mainly depends on the air mass flow rate, flow configuration (i.e. cross or counter), fiber length, fiber diameter, packing density, and the membrane's modulus of elasticity.

Zhang et al. [186] studied the effect of flow maldistribution on the deterioration in performance of a cross-flow hollow-fiber LAMEE, used for air humidification applications. A mathematical model was developed and validated with experimental results. The impact of flow maldistribution on the sensible and latent effectivenesses was tested in two identical LAMEEs with different packing densities at the same operating conditions. A deterioration factor was used to determine the effect of flow maldistribution on the LAMEE effectiveness. Fig. 41 shows that the deterioration factor for the sensible and latent effectivenesses due to flow maldistribution increased as the packing fraction decreased or as the air flow rate increased. Depending on the air flow rate and packing fraction, the sensible and latent effectivenesses decreased by 3–30% and 26–58%; respectively.

Li and Zhang [187] studied the influences of flow maldistribution on the deterioration in performance of a counter-flow hollow-fiber LAMEE, used for air humidification/dehumidification applications. Fig. 42 shows the velocity contours in the counter-flow hollow-fiber LAMEE. The degradations in the sensible and latent effectivenesses versus the air volumetric flow rate for several packing fractions (i.e. 0.1, 0.2, and 0.3) of the counter-flow hollow-fiber LAMEE are shown in Fig. 43. It is clear that the degradations in the sensible and latent effectivenesses decreased with the increase of the packing fraction. However, they found that increasing the packing fraction beyond 0.3 will not cause a significant reduction in the deterioration factor but will increase the pressure drop, thus it was recommended to design hollow-fiber LAMEEs with packing fractions of 0.3.

In conclusion, Zhang et al. [186,187] reported that compared to sensible heat exchangers, the flow maldistribution has a much more significant impact on the performance deterioration in membrane energy exchangers.

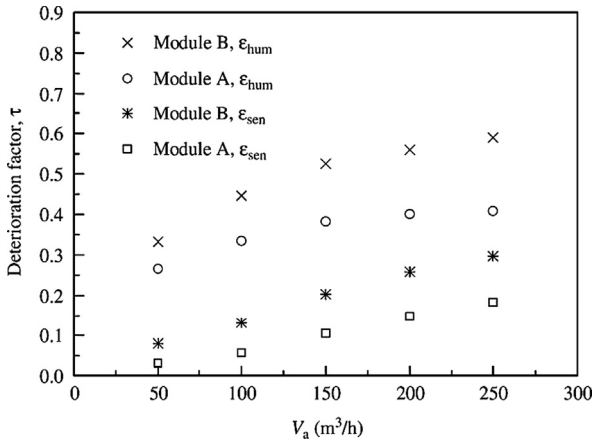

Fig. 41. Variation of deterioration factor in sensible and latent effectivenesses versus air flow rate [186].

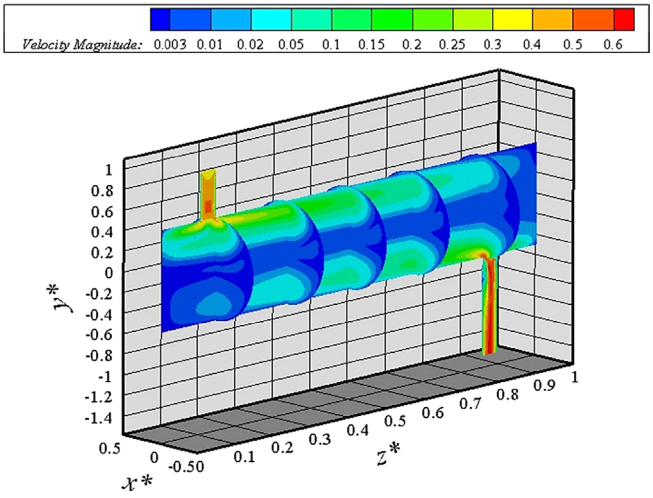

Fig. 42. Velocity contours in the counter-flow hollow-fiber LAMEE (inlet volumetric flow rate of air=0.1 m³/h and ϕ=0.3) [187].

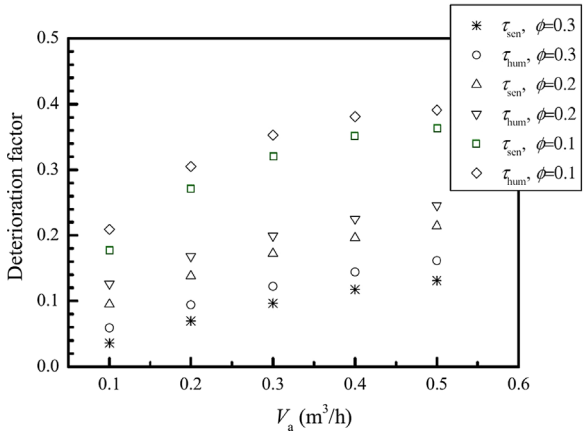

Fig. 43. Variation of deterioration factor of sensible and latent effectivenesses versus air flow rate for several packing fractions of a counter-flow hollow-fiber LAMEE [187].

9.3. Flow maldistribution in RAMEEs

Since the RAMEE system [81] mainly composes of two LAMEEs, the flow maldistribution of LAMEE would impact the performance of

the RAMEE system. Hemingson et al. [188] theoretically investigated the effect of flow maldistribution on a RAMEE performance. They found that at 30% peak membrane deflection of nominal air channel thickness and *NTU* of 12, the sensible, latent, and total effectivenesses of the RAMEE were reduced by 29%, 21%, and 25%, respectively.

10. Conclusions

The current paper presents a comprehensive review of the design, performance, and development of liquid-to-air membrane energy exchangers (LAMEEs). Based on the current review, the following conclusions are made:

1. The effectiveness of different types of LAMEEs for air cooling and dehumidifying ranged between 60% and 94%.
2. The effectiveness of a flat-plate LAMEE is higher during summer operating conditions than during winter operating conditions.
3. Flow maldistribution can significantly reduce the performance of LAMEEs.
4. Despite the fact that the hollow-fiber LAMEE has an area density per unit volume much higher than that of the flat-plate LAMEE, the flat-plate LAMEE is more feasible in practical applications for the following reasons:
   a. Hollow-fiber LAMEEs suffer from large pressure drops on the air and liquid sides.
   b. Due to the large number of the hollow fibers, if any leakage happens, it is difficult to detect the location of the leakage and fix it.
5. Compared to direct-contact liquid desiccant energy exchangers, LAMEEs eliminate the problem of desiccant droplet carry-over to the air stream.

11. Suggested topics for future research

Since LAMEEs are still new energy exchangers under development, much research is still needed. Based on the current review, the following are some recommendations for future research:

1. The effect of flow maldistribution on the performance of a flat-plate LAMEE. This could be evaluated by numerical simulations when the flow maldistribution is considered. It might be experimentally tested by using a LAMEE with a transparent cover and using the laser technology to measure the deflections of different parts of the membrane.
2. The effect of buoyancy forces on the performance of a flat-plate LAMEE. This can be done by measuring the velocity and temperature at different heights in the solution channel.
3. The effect of crystallization of the desiccant solution on the performances of a flat-plate LAMEE and a hollow-fiber LAMEE when used for diluted desiccant solution regeneration.
4. The operating conditions at which crystallization will occur in the membrane of a flat-plate LAMEE.
5. The performance of a flat-plate LAMEE for diluted desiccant solution regeneration.
6. The transient performance of a hollow-fiber LAMEE.
7. The performance of a hollow-fiber LAMEE for diluted desiccant solution regeneration.
8. A comparison between the performance (i.e. effectiveness and pressure drop) of a flat-plate and a hollow-fiber LAMEE under the same operating conditions.
9. The effect of the membrane properties on the performance of a LAMEE.
10. Developing new membranes with better properties to achieve higher effectiveness.
11. The ability of LAMEEs to remove pollutants (e.g. CO_2, CO, SO_x, NO_x, VOCs, Toluene, and Formaldehyde), from process air during the heat and moisture transfer processes.
12. Comparison between the performances of a direct-contact liquid desiccant packed bed and a LAMEE under the same operating conditions.

Acknowledgment

The authors would like to thank the *Natural Sciences and Engineering Research Council of Canada (NSERC)* for financial support.

References

[1] British petroleum statistical review of world energy ⟨bp.com/statisticalreview⟩; June 2009.
[2] British petroleum statistical review of world energy ⟨bp.com/statisticalreview⟩; June 2012.
[3] ENPI – Neighbourhood – Mediterranean & Eastern Europe, "Identification Mission for the Mediterranean Solar Plan", Final Report, January 2010, FWC beneficiaries Lot 4 – No. 2008/168828; January 2010. ⟨http://ec.europa.eu/energy/international/international_cooperation/doc/2010_01_solar_plan_report.pdf⟩.
[4] ⟨http://oee.nrcan.gc.ca/corporate/statistics/neud/dpa/showTable.cfm?type=HB&sector=aaa&juris=ca&rn=2&page=6&CFID=30286177&CFTOKEN=1e4962d1f111b44c-AA3B7047-9276-078E-875007B660714222⟩.
[5] World energy outlook 2012: executive summary, International energy agency, IEA ⟨http://www.worldenergyoutlook.org⟩; 2012.
[6] Omer AM. Energy, environment and sustainable development. Renew Sustain Energy Rev 2008;12:2265–300.
[7] Kolokotsa D, Rovas D, Kosmatopoulos E, Kalaitzakis K. A roadmap towards intelligent net zero- and positive-energy buildings. Solar Energy 2011;85:3067–84.
[8] Wyon DP. The effects of indoor air quality on performance and productivity. Indoor Air 2004;14:92–101.
[9] Al-Abidi AA, Mat SB, Sopian K, Sulaiman MY, Lim CH, Abdulrahman Th. Review of thermal energy storage for air conditioning systems. Renew Sustain Energy Rev 2012;16:5802–19.
[10] Hao X, Zhu C, Lin Y, Wang H, Zhang G, Chen Y. Optimizing the pad thickness of evaporative air-cooled chiller for maximum energy saving. Energy Build 2013;61:146–52.
[11] Awbi HB. Chapter 7 – Ventilation. Renew Sustain Energy Rev 1998;2:157–88.
[12] Spengler JD, Sexton K. Indoor air pollution: a public health perspective. Science 1983;221(no. 4605):9–17 (July).
[13] Dimitroulopoulou C. Ventilation in European dwellings: a review. Building Environ 2012;47:109–25.
[14] Simonson C. Energy consumption and ventilation performance of a naturally ventilated ecological house in a cold climate. Energy Build 2005;37:23–35.
[15] Abdel-Salam AH, Simonson CJ. Annual evaluation of energy, environmental and Economic performances of a membrane liquid desiccant air conditioning system with/without ERV. Appl Energy 2014;116:134–48.
[16] Abdel-Salam AH, Ge G, Simonson CJ. Performance analysis of a membrane liquid desiccant air-conditioning system. Energy Build 2013;62:559–69.
[17] Stritih U, Butala V. Experimental investigation of energy saving in buildings with PCM cold storage. Int J Refrig 2010;33:1676–83.
[18] Abdel-Salam AH, Ge G, Simonson CJ. Thermo-economic performance of a solar membrane liquid desiccant air conditioning system. Solar Energy 2014;102:56–73.
[19] Budaiwi I, Abdou A. HVAC system operational strategies for reduced energy consumption in buildings with intermittent occupancy: the case of mosques. Energy Conver Manag 2013;73:37–50.
[20] Kusiak A, Xu G. Modeling and optimization of HVAC systems using a dynamic neural network. Energy 2012;42:241–50.
[21] Boixo S, Diaz-Vicente M, Colmenar A, Castro MA. Potential energy savings from cool roofs in spain and andalusia. Energy 2012;38:425–38.
[22] Schulze T, Eicker U. Controlled natural ventilation for energy efficient buildings. Energy Build 2013;56:221–32.
[23] Wang L, Greenberg S, Fiegel J, Rubalcava A, Earni S, Pang X, et al. Monitoring-based HVAC commissioning of an existing office building for energy efficiency. Appl Energy 2013;102:1382–90.
[24] Haniff MF, Selamat H, Yusof R, Buyamin S, Ismail FS. Review of HVAC scheduling techniques for buildings towards energy-efficient and cost-effective operations. Renew Sustain Energy Rev 2013;27:94–103.
[25] Menassa CC, Taylor N, Nelson J. Optimizing hybrid ventilation in public spaces of complex buildings – a case study of the Wisconsin Institutes for discovery. Build Environ 2013;61:57–68.
[26] Zhang LZ, Jiang Y. Heat and mass transfer in a membrane-based energy recovery ventilator. J Membr Sci 1999;163:29–38.

[27] Niu JL, Zhang LZ. Membrane-based enthalpy exchanger: material considerations and clarification of moisture resistance. J Membr Sci 2001;189:179–91.
[28] Zhang LZ, Niu JL. Effectiveness correlations for heat and moisture transfer processes in an enthalpy exchanger with membrane cores. ASME J Heat Transf 2002;124:922–9.
[29] Zhang LZ. Investigation of moisture transfer effectiveness through a hydrophilic polymer membrane with a field and laboratory emission cell. Int J Heat Mass Transf 2006;49:1176–84.
[30] Zhang LZ. Heat and mass transfer in a cross-flow membrane-based enthalpy exchanger under naturally formed boundary conditions. Int J Heat aMass Transf 2007;50:151–62.
[31] Zhang LZ. Numerical study of heat and mass transfer in an enthalpy exchanger with a hydrophobic–hydrophilic composite membrane core. Numer Heat Transf, Part A: Appl, An Int. J. Comput. Methodol. 2007;51(7):697–714.
[32] Zhang LZ. Heat and mass transfer in plate-fin sinusoidal passages with vapor-permeable wall materials. Int. J. Heat Mass Transf 2008;51:618–29.
[33] Zhang LZ, Liang CH, Pei LX. Heat and moisture transfer in application scale parallel-plates enthalpy exchangers with novel membrane materials. J Membr Sci 2008;325:672–82.
[34] Zhang LZ. Total heat recovery: heat and moisture recovery from ventilation air. New York: Nova Science Publishing Co.; 2008.
[35] Zhang LZ. Flow maldistribution and performance deteriorations in membrane-based heat and mass exchangers. ASME J Heat Transf 2009;131(111801-1 to 111801-7).
[36] Liu S, Riffat S, Zhao X, Yuan Y. Impact of adsorbent finishing and absorbent filming on energy exchange efficiency of an air-to-air cellulose fibre heat & mass exchanger. Build Environ 2009;44:1803–9.
[37] Zhang LZ. Heat and mass transfer in plate-fin enthalpy exchangers with different plate and fin materials. Int J Heat Mass Transf 2009;52:2704–13.
[38] Zhang LZ. Performance deteriorations from flow maldistribution in air-to-air heat exchangers: a parallel-plates membrane core case. Numer Heat Transf, Part A: Appl, An Int J Comput Methodol, 56:9 2009:746–63.
[39] Zhang LZ, Liang CH, Pei LX. Conjugate heat and mass transfer in membrane-formed channels in all entry regions. Int J Heat Mass Transf 2010;53:815–24.
[40] Zhang LZ. Heat and mass transfer in a quasi-counter flow membrane-based total heat exchanger. Int J Heat Mass Transf 2010;53:5478–86.
[41] Min J, Su M. Performance analysis of a membrane-based enthalpy exchanger: effects of the membrane properties on the exchanger performance. J Membr Sci 2010;348:376–82.
[42] Min J, Su M. Performance analysis of a membrane-based energy recovery ventilator: effects of membrane spacing and thickness on the ventilator performance. Appl Therm Eng 2010;30:991–7.
[43] Zhang LZ. An analytical solution for heat mass transfer in a hollow fiber membrane based air-to-air heat mass exchanger. J Membr Sci 2010;360:217–25.
[44] Min J, Su M. Performance analysis of a membrane-based energy recovery ventilator: Effects of outdoor air state. Appl Therm Eng 2011;31:4036–43.
[45] Aarnes SM. Membrane based heat exchanger. (M.Sc. Thesis in Product Design and Manufacturing, Department of Energy and Process Engineering). Norway: Norwegian University of Science and Technology; 2012.
[46] Yaïci W, Ghorab M, Entchev E. Numerical analysis of heat and energy recovery ventilators performance based on cfd for detailed design. Appl Therm Eng 2013;51:770–80.
[47] Min J, Wang L. Coupled heat and mass transfer during moisture exchange across a membrane. J Membr Sci 2013;430:150–7.
[48] Woods J, Kozubal E. Heat transfer and pressure drop in spacer-filled channels for membrane energy recovery ventilators. Appl Therm Eng 2013;50:868–76.
[49] Besant RW, Simonson CJ. Air-to-air energy recovery. ASHRAE J 2000:31–8 (May).
[50] Zhang Y, Jiang Y, Zhang LZ, Deng Y, Jin Z. Analysis of thermal performance and energy savings of membrane based heat recovery ventilator. Energy 2000;25:515–27.
[51] Zhang LZ, Niu JL. Energy requirements for conditioning fresh air and the long-term savings with a membrane-based energy recovery ventilator in Hong Kong. Energy 2001;26:119–35.
[52] Zhang LZ, Zhu DS, Deng XH, Hua B. Thermodynamic modeling of a novel air dehumidification system. Energy Build 2005;37:279–86.
[53] Nasif M, AL-Waked R, Morrison G, Behnia M. Membrane heat exchanger in HVAC energy recovery systems, systems energy analysis. Energy Build 2010;42:1833–40.
[54] Liang CH, Zhang LZ, Pei LX. Performance analysis of a direct expansion air dehumidification system combined with membrane-based total heat recovery. Energy 2010;35:3891–901.
[55] Ge G, Xiao F, Xu X. Model-based optimal control of a dedicated outdoor air-chilled ceiling system using liquid desiccant and membrane-based total heat recovery. Appl Energy 2011;88:4180–90.
[56] Radhwan AM, Gari HN, Elsayed MM. Parametric study of a packed bed dehumidifier/regenerator using $CaCl_2$ liquid desiccant. Renew Energy 1993;3:49–60.
[57] Daou K, Wang RZ, Xia ZZ. Desiccant cooling air conditioning: a review. Renew Sustain Energy Rev 2006;10:55–77.
[58] Mei L, Dai YJ. A technical review on use of liquid-desiccant dehumidification for air-conditioning application. Renew Sustain Energy Rev 2008;12:662–89.
[59] Martin V, Goswami DY. Effectiveness of heat and mass transfer processes in a packed bed liquid desiccant dehumidifier/regenerator. HVAC&R Res 2000;6(1):21–39.
[60] Dai YJ, Wang RZ, Zhang HF, Yu JD. Use of liquid desiccant cooling to improve the performance of vapour compression air conditioning. Appl Therm Eng 2001;21:1185–202.
[61] Pietruschka D, Eicker U, Huber M, Schumacher J. Experimental performance analysis and modelling of liquid desiccant cooling systems for air conditioning in residential buildings. Int J Refrig 2006;29:110–24.
[62] Liu XH, Jiang Y, Chang XM, Yi XQ. Experimental investigation of the heat and mass transfer between air and liquid desiccant in a cross-flow regenerator. Renew Energy 2007;32:1623–36.
[63] Yin Y, Zhang X, Chen Z. Experimental study on dehumidifier and regenerator of liquid desiccant cooling air conditioning system. Build Environ 2007;42:2505–11.
[64] Liu XH, Jiang Y. Handling zone dividing method in packed bed liquid desiccant dehumidification/regeneration process. Energy Conver Manag 2009;50:3024–34.
[65] Tu M, Ren CQ, Zhang LA, Shao JW. Simulation and analysis of a novel liquid desiccant air-conditioning system. Appl Therm Eng 2009;29:2417–25.
[66] Longo GA, Gasparella A. Experimental analysis on desiccant regeneration in a packed column with structured and random packing. Solar Energy 2009;83:511–21.
[67] Enteria N, Yoshino H, Mochida A. Review of the advances in open-cycle absorption air-conditioning systems. Renew Sustain Energy Rev 2013;28:265–89.
[68] Wang L, Li N, Zhao B. Exergy performance and thermodynamic properties of the ideal liquid desiccant dehumidification system. Energy Build 2010;42:2437–44.
[69] Tu M, Ren CQ, Tang GF, Zhao ZS. Performance comparison between two novel configurations of liquid desiccant air-conditioning system. Building Environ 2010;45:2808–16.
[70] Zhang L, Dang C, Hihara E. Performance analysis of a no-frost hybrid air conditioning system with integrated liquid desiccant dehumidification. Int J Refrig 2010;33:116–24.
[71] Wang X, Cai W, Lu J, Sun Y, Ding X. A hybrid dehumidifier model for real-time performance monitoring, control and optimization in liquid desiccant dehumidification system. Appl Energy 2013;111:449–55.
[72] Luo Y, Yang H, Lu L. Liquid desiccant dehumidifier: Development of a new performance predication model based on CFD. Int J Heat Mass Transf 2014;69:408–16.
[73] Li XW, Zhang XS, Cao RQ, Quan S. Progress in selecting desiccant and dehumidifier for liquid desiccant cooling system. Energy Build 2012;49:410–8.
[74] Mohammad AT, Mat SB, Sulaiman MY, Sopian K, Al-abidi AA. Implementation and validation of an artificial neural network for predicting the performance of a liquid desiccant dehumidifier. Energy Conver Manag 2013;67:240–50.
[75] Li XW, Zhang XS, Wang F. A kinetic mass transfer model of liquid dehumidification for liquid desiccant cooling system. Energy Build 2013;61:93–9.
[76] Luo Y, Yang H, Lu L, Qi R. A review of the mathematical models for predicting the heat and mass transfer process in the liquid desiccant dehumidifier. Renew Sustain Energy Rev 2014;31:587–99.
[77] Mohammad AT, Mat SB, Sulaiman MY, Sopian K, Al-abidi AA. Survey of hybrid liquid desiccant air conditioning systems. Renew Sustain Energy Rev 2013;20:186–200.
[78] Mardiana-Idayu A, Riffat SB. Review on heat recovery technologies for building applications. Renew Sustain Energy Rev 2012;16:1241–55.
[79] Alonso MJ, Mathisen HM, Novakovic V, Simonson CJ. Review of air-to-air heat/energy exchangers for use in NZEBs in the Nordic countries, In: Proceedings of the second international conference on building energy and environment “COBEE2012”, Boulder, Colorado, USA; 1st–4th August, 2012.
[80] Zhang LZ. Progress on heat and moisture recovery with membranes: from fundamentals to engineering applications. Energy Conver Manag 2012;63:173–95.
[81] Ge G, Abdel-Salam MRH, Besant RW, Simonson CJ. Research and applications of liquid-to-air membrane energy exchangers in building HVAC systems at University of Saskatchewan: a review. Renew Sustain Energy Rev 2013;26:464–79.
[82] Mohammad AT, Mat SB, Sulaiman MY, Sopian K, Al-abidi AA. Survey of liquid desiccant dehumidification system based on integrated vapor compression technology for building applications. Energy Build 2013;62:1–14.
[83] Abdel-Salam MRH, Fauchoux M, Ge G, Besant RW, Simonson CJ. Expected energy and economic benefits, and environmental impacts for liquid-to-air membrane energy exchangers (LAMEEs) in HVAC systems: A review. Appl Energy 2014;127:202–18.
[84] Mahmud K. Design and performance testing of counter-cross-flow run-around membrane energy exchanger system. (M.Sc. thesis). Saskatoon, Saskatchewan, Canada: Department of Mechanical Engineering, College of Engineering, University of Saskatchewan; 2009.
[85] ASHRAE Handbook 2004, HVAC systems and equipment, American society of heating, refrigerating and air-conditioning engineers, Inc.
[86] Vali A, Simonson CJ, Besant RW, Mahmood G. Numerical model and effectiveness correlations for a run-around heat recovery system with combined counter and cross flow exchangers. Int J Heat Mass Transf 2009;52:5827–40.
[87] Isetti C, Nannei E, Magrini A. On the application of a membrane air–liquid contactor for air dehumidification. Energy Build 1997;25:185–93.

[88] Wickramasinghe SR, Semmens MJ, Cussler EL. Better hollow fiber contactors. J Membr Sci 1991;62:371–88 (Cited in Ref. [87]).
[89] Zhang LZ. An analytical solution to heat and mass transfer in hollow fiber membrane contactors for liquid desiccant air dehumidification. ASME J Heat Transf 2011;133(9):092001.1–8.
[90] Zhang LZ, Huang SM, Pei LX. Conjugate heat and mass transfer in a cross-flow hollow fiber membrane contactor for liquid desiccant air dehumidification. Int J Heat Mass Transf 2012;55:8061–72.
[91] Zhang LZ, Huang SM, Chi JH, Pei LX. Conjugate heat and mass transfer in a hollow fiber membrane module for liquid desiccant air dehumidification: a free surface model approach. Int J Heat Mass Transf 2012;55:3789–99.
[92] ANSI/ASHRAE STANDARD 84-2008, Method of test for air-to-air heat/energy exchangers, American society of heating, refrigerating, and air-conditioning engineers, Atlanta.
[93] Simonson CJ, Besant RW. Energy wheel effectiveness: Part I-Development of dimensionless groups. Int J Heat Mass Transf 1999;42:2161–70.
[94] Hemingson H. The impacts of outdoor air conditions and non-uniform exchanger channels on a run-around membrane energy exchanger. (M. Sc. thesis). Saskatoon, Saskatchewan, Canada: Department of Mechanical Engineering, College of Engineering, University of Saskatchewan; 2010.
[95] Zhang LZ. Coupled heat and mass transfer in an application-scale cross-flow hollow fiber membrane module for air humidification. Int J Heat Mass Transf 2012;55:5861–9.
[96] Zhang LZ, Huang SM. Coupled heat and mass transfer in a counter flow hollow fiber membrane module for air humidification. Int J Heat Mass Transf 2011;54:1055–63.
[97] Woods J. Membrane processes for heating, ventilation, and air conditioning. Renew Sustain Energy Rev 2014;33:290–304.
[98] MEMBRANA Company, ⟨http://www.membranafiltration.com/filtration-membranes/hydrophobic-vs-hydrophilic.cfm⟩ [accessed 03.05.13].
[99] Khayet M. Membranes and theoretical modeling of membrane distillation: a review. Adv Colloid Interface Sci 2011;164:56–88.
[100] Zhang XR, Zhang LZ, Liu HM, Pei LX. One-step fabrication and analysis of an asymmetric cellulose acetate membrane for heat and moisture recovery. J Membr Sci 2011;366:158–65.
[101] Zhang LZ. Fabrication of a lithium chloride solution based composite supported liquid membrane and its moisture permeation analysis. J Membr Sci 2006;276:91–100.
[102] Zhang LZ, Xiao F. Simultaneous heat and moisture transfer through a composite supported liquid membrane. Int J Heat Mass Transf 2008;51:2179–89.
[103] Larson MD, Simonson CJ, Besant RW, Gibson PW. The elastic and moisture transfer properties of polyethylene and polypropylene membranes for use in liquid-to-air energy exchangers. J Membr Sci 2007;302:136–49.
[104] Larson MD. The performance of membranes in a newly proposed runaround heat and moisture exchanger. (M.Sc. Thesis). Saskatoon, Saskatchewan, Canada: Department of Mechanical Engineering, College of Engineering, University of Saskatchewan; 2006.
[105] Khayet M, Matsuura T. Preparation and characterization of polyvinylidene fluoride membranes for membrane distillation. Ind Eng Chem Res 2001;40:5710–8.
[106] Smolders K, Franken ACM. Terminology for membrane distillation. Desalination 1989;Vol. 72:249–62 (Cited in Ref. [105]).
[107] Iversen SB, Bhatia VK, Dam-Johansen K, Jonsson G. Characterization of microporous membranes for use in membrane contactors. J Membr Sci 1997;130:205–17.
[108] Mackie JS, Meares P. In: Proceedings of the royal society, A232, 498; 1955. [Cited in Ref. [107]].
[109] Brandrup J, Immergut EH. Polymer handbook. 3rd ed.. New York: Wiley; 1989.
[110] Harper CA. Handbook of Plastics, Elastomers and Composites. 3rd ed.. New York: McGraw-Hill; 1996.
[111] Van Kreveleh DW. Properties of Polymers. 3rd ed.. Amsterdam: Elsevier; 1990.
[112] Phattaranawik J, Jiraratananon R, Fane AG. Heat transport and membrane distillation coefficients in direct contact membrane distillation. J Membr Sci 2003;212:177–93.
[113] Beriault DA. Run-around membrane energy exchanger prototype 4 design and laboratory testing. (M.Sc. Thesis). Saskatoon, Saskatchewan, Canada: Department of Mechanical Engineering, College of Engineering, University of Saskatchewan; 2011.
[114] Zhang LZ, Zhang XR, Miao QZ, Pei LX. Selective permeation of moisture and VOCs through polymer membranes used in total heat exchangers for indoor air ventilation. Indoor Air 2012;22:321–30.
[115] Isetti C, Magrini A, Nannei E. The application of vapour-permeable synthetic membranes to the climatic stabilization of museum showcases. Stud Conserv 1996;Vol. 41:229–40.
[116] Bergero S, Chiari A, Isetti C. On the performance of a plane plate membrane contactor for air dehumidification, In: Proceedings of CLIMA 2000/Napoli 2001 World Congress-Napoli (I), Italy; 15–18 September, 2001.
[117] Bergero S, Chiari A. Passive hygrometric control of confined environments by means of membrane contactors and hygroscopic solutions, In: Proceedings of the 5th international congress on energy, environment and technological innovation (EETI) 2004, Riocentro, Rio de Janeiro, Brazil; 4–7 October, 2004.
[118] Vestrelli F. Study on membrane contactors: performances analysis, system simulations and fields of application. (Ph.D. thesis "Doctorate of Philosophy in Technical Physics"). Genoa, Italy: Faculty of Engineering, University of Genoa; 2006.
[119] Fan H. Modeling a run-around heat and moisture recovery system. (M.Sc. thesis). Saskatoon, Saskatchewan, Canada: Department of Mechanical Engineering, College of Engineering, University of Saskatchewan; 2005.
[120] Fan H, Simonson CJ, Besant RW, Shang W. Performance of a run-around system for HVAC heat and moisture transfer applications using cross-flow plate exchangers coupled with aqueous lithium bromide. HVAC&R Res 2006; Vol. 12:313–36.
[121] Seyed-Ahmadi M. Modeling the transient behavior of a run-around heat and moisture exchanger system. (M.Sc. thesis). Saskatoon, Saskatchewan, Canada: Department of Mechanical Engineering, College of Engineering, University of Saskatchewan; 2008.
[122] Seyed-Ahmadi M, Erb B, Simonson CJ, Besant RW. Transient behavior of run-around heat and moisture exchanger system; part I: model formulation and verification. Int J Heat Mass Transf 2009;52:6000–11.
[123] Seyed-Ahmadi M, Erb B, Simonson CJ, Besant RW. Transient behavior of run-around heat and moisture exchanger system; Part II: Sensitivity studies for a range of initial conditions. Int J Heat Mass Transf 2009;52:6012–20.
[124] Vali A. Modeling a run-around heat and moisture exchanger using two counter/cross flow exchangers. (M.Sc. thesis). Saskatoon, Saskatchewan, Canada: Department of Mechanical Engineering, College of Engineering, University of Saskatchewan; 2009.
[125] Hemingson HB, Simonson CJ, Besant RW. Steady-state performance of a run-around membrane energy exchanger (RAMEE) for a range of outdoor air conditions. Int J Heat Mass Transf 2011;54:1814–24.
[126] Namvar R, Pyra D, Ge G, Simonson CJ, Besant RW. Transient characteristics of a liquid-to-air membrane energy exchanger (LAMEE) experimental data with correlations. Int J Heat Mass Transf 2012;55:6682–94.
[127] Namvar R, Ge G, Simonson CJ, Besant RW. Transient heat and moisture transfer characteristics of a liquid-to-air membrane energy exchanger (LAMEE) model verification and extrapolation. Int J Heat Mass Transf 2013;66:757–71.
[128] Hemingson H. Preliminary testing for run around heat and moisture exchanger. (Summer Work report). Saskatoon, Saskatchewan, Canada: Department of Mechanical Engineering, College of Engineering, University of Saskatchewan; 2005.
[129] Erb B. Run-around membrane energy exchanger performance and operational control strategies. (M.Sc. thesis). Saskatoon, Saskatchewan, Canada: Department of Mechanical Engineering, College of Engineering, University of Saskatchewan; 2009.
[130] Erb B, Seyed-Ahmadi M, Simonson CJ, Besant RW. Experimental measurements of a run-around membrane energy exchanger (RAMEE) with comparison to a numerical model. ASHRAE Trans 2009;Vol. 115:689–705.
[131] Mahmud K, Mahmood GI, Simonson CJ, Besant RW. Performance testing of a counter-cross-flow run-around membrane energy exchanger (RAMEE) system for HVAC applications. Energy Build 2010;42:1139–47.
[132] Moghaddam DG, LePoudre P, Ge G, Besant RW, Simonson CJ. Small-scale single-panel liquid-to-air membrane energy exchanger (LAMEE) test facility development, commissioning and evaluating the steady-state performance. Energy Build 2013;66:424–36.
[133] Ge G, Moghaddam DG, Namvar R, Simonson CJ, Besant RW. Analytical model based performance evaluation, sizing and coupling flow optimization of liquid desiccant run-around membrane energy exchanger systems. Energy Build 2013;62:248–57.
[134] AHRI Standard 1060, Performance rating for air-to-air exchangers for energy recovery ventilation equipment, Arlington, VA: Air-Conditioning & Refrigeration Institute; 2005.
[135] Incropera FP, Dewitt DP. Fundamentals of heat and mass transfer. 5th ed.. New York: John Wiley & Sons; 2002.
[136] Nasif MS, Morrison GL, Behnia M. Heat and mass transfer in air to air enthalpy heat exchangers, In: Proceedings of the 6th world conference on experimental heat transfer, fluid mechanics and thermodynamics, Matsushima, Miyagi, Japan; 2005.
[137] Moghaddam DG, LePoudre P, Besant RW, Simonson CJ. Steady-state performance of a small-scale liquid-to-air membrane energy exchanger for different heat and mass transfer directions, and liquid desiccant types and concentrations: experimental and numerical data. ASME J Heat Transf 2013;135:1–13.
[138] Moghaddam DG, LePoudre P, Besant RW, Simonson CJ. Evaluating the steady-state performance of a small-scale single-panel liquid-to-air membrane energy exchanger (LAMEE) under summer AHRI test conditions, CLIMA 2013, In: Proceedings of the 11th REHVA world congress & 8th international conference on IAQVEC, Prague congress center, Prague, Czech Republic; 16–19 June, 2013.
[139] Moghaddam DG, Ge G, Abdel-Salam AH, Besant RW, Simonson CJ. Effects of solution inlet temperature on the effectiveness and moisture removal rate of a liquid-to-air membrane energy exchanger (LAMEE) during regenerator operating conditions, In: Proceedings of the 24th CANCAM, Saskatoon, Saskatchewan, Canada; 2nd–6th June, 2013.
[140] Afshin M. Selection of the liquid desiccant in a run-around membrane energy exchanger. (M.Sc. thesis). Saskatoon, Saskatchewan, Canada: Department of Mechanical Engineering, College of Engineering, University of Saskatchewan; 2010.
[141] Fumo N, Goswami DY. Study of an aqueous lithium chloride desiccant system: Air dehumidification and desiccant regeneration. Solar Energy 2002;72:351–61.
[142] Liu XH, Jiang Y, Yi XQ. Effect of regeneration mode on the performance of liquid desiccant packed bed regenerator. Renew Energy 2009;34:209–16.

[143] Jain S, Tripathi S, Das Rajat S. Experimental performance of a liquid desiccant dehumidification system under tropical climates. Energy Conver Manag 2011;Vol. 52:2461–6.
[144] Moghaddam DG, Mahmood G, Ge G, Bolster J, Besant RW, Simonson CJ. Steady-state performance of a prototype (200 CFM) liquid-to-air membrane energy exchanger (LAMEE) under summer and winter test conditions, In: Proceedings of the ASME 2013 Summer Heat Transfer Conference, Minneapolis, MN, USA; 14th–19th July, 2013.
[145] Abdel-Salam AH, Ge G, Fauchoux MT, Moghaddam DG, Simonson CJ. Effectiveness evaluation of a liquid-to-air membrane energy exchangers as dehumidifier/regenerator in a liquid desiccant air-conditioning system, In: Proceedings of the 24th CANCAM, Saskatoon, Saskatchewan, Canada; June 2–6, 2013.
[146] Huang SM, Zhang LZ, Tang K, Pei LX. Fluid flow and heat mass transfer in membrane parallel-plates channels used for liquid desiccant air dehumidification. Int J Heat Mass Transf 2012;55:2571–80.
[147] Huang SM, Zhang LZ, Yang M. Conjugate heat and mass transfer in membrane parallel-plates ducts for liquid desiccant air dehumidification: effects of the developing entrances. J Membr Sci 2013;437:82–9.
[148] Teertstra P, Culham JR, Yovanovich MM. Comprehensive review of natural and mixed convection heat transfer models for circuit board arrays. J Electr Manuf 1997;7(2):79–92 (Cited in Ref. [127]).
[149] Yao LS. Free and forced convection in the entry region of a heated vertical channel. Int J Heat Mass Transf 1983;26:65–72 (Cited in Ref. [127]).
[150] Bergero S, Chiari A. Experimental and theoretical analysis of air humidification/dehumidification processes using hydrophobic capillary contactors. Appl Therm Eng 2001;21:1119–35.
[151] Chiari A. Air humidification with membrane contactors: Experimental and theoretical results. Int J Ambient Energy, 21:4 2000:187–95.
[152] Zhang LZ. Heat and mass transfer in a randomly packed hollow fiber membrane module: a fractal model approach. Int J Heat Mass Transf 2011; Vol. 54:2921–31.
[153] Incropera FP, Dewitt DP. Introduction to heat transfer. 3rd ed.. New York: John Wiley Sons; 1996 (Cited in Ref. [90]).
[154] Kays WM, London AL. Compact heat exchangers. New York: McGraw-Hill, Inc.; 1984 (Cited in Ref. [90]).
[155] Kays WM, Crawford ME. Convective heat and mass transfer. New York: McGraw-Hill, Inc.; 1993 (Cited in Ref. [90]).
[156] Frank K, Mark SB. Principles of heat transfer. 4th ed.. New York: Harper & Row Publishers, Inc.; 1986 (Cited in Ref. [157]).
[157] Huang SM, Zhang LZ, Kai Tang, Pei LX. Turbulent heat and mass transfer across a hollow fiber membrane tube bank in liquid desiccant air dehumidification. ASME J Heat Transf 2012;134:1–10 (August).
[158] Jones WP, Launder BE. The prediction of laminarization with a two-equation model of turbulence. Int J Heat Mass Transf 1972;15(2):301–11 (Cited in Ref. [157]).
[159] Jones WP, Launder BE. The prediction of low-Reynolds- number phenomena with two-equation model of turbulence. Int J Heat Mass Transf 1973;16 (6):1119–30 (Cited in Ref. [157]).
[160] Zhang LZ, Li ZX. Convective mass transfer and pressure drop correlations for cross-flow structured hollow fiber membrane bundles under low Reynolds numbers but with turbulent flow behaviors. J Membr Sci 2013;434:65–73.
[161] Zhang LZ. Conjugate heat and mass transfer in heat mass exchanger ducts. 1st ed. New York: Academic Press, Elsevier; 2013.
[162] Grimison ED. Correlation and utilization of new data on flow resistance and heat transfer for cross flow of gases over tube banks. ASME Trans 1937;59:583–94.
[163] Zukauskas A. Heat transfer from tubes in cross flow. Adv Heat Transf 1972;8:93–160.
[164] Hausen H. Heat transfer in counter flow, parallel flow and cross flow. New York: McGraw-Hill, Inc; 1983.
[165] Khan WA, Culham JR, Yovanovich MM. Convection heat transfer from tube banks in cross flow: analytical approach. Int J Heat Mass Transf 2006;49: 4831–8.
[166] Gao WZ, Shi YR, Cheng YP, Sun WZ. Experimental study on partially internally cooled dehumidification in liquid desiccant air conditioning system. Energy Build 2013;61:202–9.
[167] Khan AY. Cooling and dehumidification performance analysis of internally-cooled liquid desiccant absorbers. Appl Therm Eng 1998;18:265–81.
[168] Liu XH, Jiang Y, Qu KY. Heat and mass transfer model of cross flow liquid desiccant air dehumidifier/regenerator. Energy Conver Manag 2007;48: 546–54.
[169] Ren CQ, Tu M, Wang HH. An analytical model for heat and mass transfer processes in internally cooled or heated liquid desiccant–air contact units. Int J Heat Mass Transf 2007;50:3545–55.
[170] Yin Y, Zhang X, Wang G, Luo L. Experimental study on a new internally cooled/heated dehumidifier/regenerator of liquid desiccant systems. Int J Refrig 2008;31:857–66.
[171] Liu XH, Chang XM, Xia JJ, Jiang Y. Performance analysis on the internally cooled dehumidifier using liquid desiccant. BuildEnviron 2009;44:299–308.
[172] Yin Y, Zhang X, Peng D, Li X. Model validation and case study on internally cooled/heated dehumidifier/regenerator of liquid desiccant systems. Int J Therm Sci 2009;48:1664–71.
[173] Yin Y, Zhang X. Comparative study on internally heated and adiabatic regenerators in liquid desiccant air conditioning system. Build Environ 2010;Vol. 45:1799–807.
[174] Bansal P, Jain S, Moon C. Performance comparison of an adiabatic and an internally cooled structured packed-bed dehumidifier. Appl Therm Eng 2011;31:14–9.
[175] Zhang T, Liu X, Jiang J, Chang X, Jiang Y. Experimental analysis of an internally-cooled liquid desiccant dehumidifier. Build Environ 2013;63:1–10.
[176] Qi R, Lu L, Yang H. Development of simplified prediction model for internally cooled/heated liquid desiccant dehumidification system. Energy Build 2013;59:133–42.
[177] Isetti C, Nannei E, Orlandini B. Three-fluid membrane contactors for improving the energy efficiency of refrigeration and air-handling systems. Int J Ambient Energy 2013. http://dx.doi.org/10.1080/01430750.2012.755905.
[178] Cabot Specialty Fluids, 2008, "Formate Technical Manual", Part A, section A2 (2011), and Part A, section A3, 2012. ⟨http://www.formatebrines.com⟩. [Cited in Ref. [177].
[179] Chin WM, Raghavan VR. On the adverse influence of higher statistical moments of flow maldistribution on the performance of a heat exchanger. Int J Therm Sci 2011;50:581–91.
[180] Kuppan T. Heat exchanger design handbook. New York: Marcel Dekker, Inc.; 2000.
[181] Mueller AC, Chiou JP. Review of various types of flow maldistribution in heat exchangers. Heat Transf Eng 1988;9(2):36–50.
[182] Mueller AC. Effects of some types of maldistribution on the performance of heat exchangers. Heat Transf Eng 1987;8(2):75–86.
[183] Lalot S, Florent P, Lang SK, Bergles AE. Flow maldistribution in heat exchangers. Appl Therm Eng 1999;Vol. 19:847–63.
[184] Elgowainy A. Effect of airflow mal-distribution on pressure drop and thermal performance of heat exchangers in residential heat pump systems. ASHRAE Trans 2003;109(2) (Article no. 4629. Cited in Ref. [179]).
[185] T'joen C, Willockx A, Steeman HJ, Paepe MD. Performance prediction of compact fin and-tube heat exchangers in maldistributed airflow. Heat Transf Eng 2007;28(12):986–96.
[186] Zhang LZ, Li ZX, Zhong TS, Pei LX. Flow maldistribution and performance deteriorations in a cross flow hollow fiber membrane module for air humidification. J Membr Sci 2013;427:1–9.
[187] Li ZX, Zhang LZ. Flow maldistribution and performance deteriorations in a counter flow hollow fiber membrane module for air humidification/dehumidification. Int J Heat Mass Transf 2014;74:421–30.
[188] Hemingson HB, Simonson CJ, Besant RW. Effects of non-uniform channels on the performance of a run-around membrane energy exchanger (RAMEE), In: Proceedings of the 12th international conference on air distribution in rooms, ROOMVENT 2011, Trondheim, Norway; 19th–22nd June, 2011.